Master's Thesis

Hydrogen gas sensor: self-heating based array of single suspended carbon nanowires decorated with palladium nanoparticles

Junyoung Seo

Department of Mechanical Engineering

Graduate School of UNIST

2017

Hydrogen gas sensor: self-heating based array of single suspended carbon nanowires decorated with palladium nanoparticles

Junyoung Seo

Department of Mechanical Engineering

Graduate School of UNIST

Hydrogen gas sensor: self-heating based array of single suspended carbon nanowires decorated with palladium nanoparticles

A Thesis/dissertation
submitted to the Graduate School UNIST
in partial fulfillment of the
requirements for the degree of
Master of Mechanical engineering

Junyoung Seo

7. 7. 2017

Approved by

Advisor

Heungjoo Shin

Hydrogen gas sensor: self-heating based array of single suspended carbon nanowires decorated with palladium nanoparticles

Junyoung Seo

The certifies that the thesis of Junyoung Seo is approved.

7. 7. 2017

signature

Advisor: Heungjoo Shin

signature

Thesis Committee member: Taesung Kim

signature

Thesis Committee member: Hoon Eui Jeong

Dedication

I dedicate this thesis to my parents who gave me endless love with a strong trust for all my life.

And I would not forget your love forever. Make each day count!

Without their love, I could not get this academic achievement.

Abstract

This study reports the development of a novel hydrogen gas sensor based on an array of single suspended carbon nanowires (Φ ~ 200 nm, length ~ 100 μm) decorated with Pd nanoparticles (PdNPs) of various sizes for room temperature H_2 gas sensing. These sensors provide high sensitivity, a wide sensing range (10 ppm − 5 %), and complete gas response recovery in 5 s with ultralow power consumption (30 μW). Such performance is achieved using a novel suspended PdNP/carbon nanowire architecture, which offers enhanced mass transfer, high surface area to volume ratios, and good thermal insulation. This platform can be fabricated using simple batch microfabrication processes including carbon-MEMS and electrodeposition. The sensitivity and range of the sensor can be modulated by controlling Pd nanoparticle sizes (3 – 5 nm PdNPs: 3.2 % $ppm^{-1/2}$, 10 − 1,000 ppm; 10 – 15 nm PdNPs: 0.32 % $ppm^{-1/2}$, 700 ppm − 5 %). A wide sensing range is achieved by integrating nanowires with various sizes of PdNPs onto a chip. The electrical resistance of a suspended PdNP/carbon nanowire quickly and completely recovers its original state in a very short time via ultralow-power, Joule heat-based self-heating. This self-heating-based system achieves reliable, continuous, and long-term H_2 detection.

Contents

1. Introduction

1.1 Necessity of hydrogen gas sensor

Hydrogen gas (hydrogen) has pulled in a step by step high consideration as another vitality source, keeping pace with the requirements to manage the expected depletion of conventional petroleum products and to reduce an a worldwide temperature alteration issue by diminishing the utilization of non-renewable energy source [1]. Focal points of hydrogen gas lie in its cleanliness, substance reactivity, recyclability, and common wealth. Nonetheless, hydrogen is exceptionally combustible and ends up noticeably unstable when its focus is surpassed more than 4% in air [2-4]. Thus, quick and solid discovery of hydrogen gas require the far reaching of hydrogen-based applications. Different trials have been performed to create hydrogen sensors with high affectability and quick reaction [5-11], and a portion of the underlying endeavors are epitomized by the officially marketed metal-oxide-semiconductor (MOS) sort [12] sensors. In any case, those sensors in early stage were experienced disadvantages, for example, high power utilization, poor gas selectivity, and high working temperatures. All the more as of late, fragile gadgets, for example, high electron versatility transistors (HEMTs) and metal-oxide-semiconductor field-impact transistors (MOSFETs) and metal-semiconductor Schottky diodes, have risen superior hydrogen detecting [13-18]. In spite of the fact that these gadgets have accomplished abundantly enhanced affectability and sensible reaction times and recognition confines, the manufacture procedures are confused, making the

gadgets exorbitant. In this circumstance, the consideration for Pd has been broadly sought after in hydrogen gas sensor field becaused of the mass exchange connection of Pd and hydrogen at room temperature operability.

1.2 Pd based hydrogen gas sensor

1.2.1 Various Pd nanomaterial types

At the point when a Pd is presented to hydrogen, hydrogen particles are adsorbed onto the Pd surface and separated into hydrogen iotas because of Pd impetus response [19]. These hydrogen molecules diffuse until they involve the interstitial locales of the Pd grid, causing a specific measure of cross section extension [20,21] and diminishing conductivity. The dispersion for the most part happens through high diffusivity ways, for example, grain limits and disengagements or through an opportunity trade system [22-23], bringing about the sum reliance of hydrogen retention. The ingested hydrogen molecules collaborate with Pd iotas to shape PdHx and increment the recurrence of scrambling occasions of charge transporters, which specifically prompts the resistance increment of the Pd. Be that as it may, as indicated by expanding hydrogen assimilation, Pd might be helpless against basic disfigurements because of PdHx stage changes. The α stage (strong arrangement of Pd and H) changes into a β stage (palladium hydride) when the hydrogen fixation increments [24].

- **Pd thin film**

Pd thin films are standard type of low dimensional Pd nanostructure, which are effectively versatile to usable hydrogen sensor applications. In these structures, the thickness of the films is typically limited to not as much as a few nanoscale (nm), while the width is adaptably fluctuated to fit into permitted measurement in the scope of a few millimeter scale (mm). The low angle proportion of film thickness to width by and large encourages hydrogen ingestion and desorption procedures, and makes the Pd film/substrate interface significantly imperative in the cyclic hydrogen detecting because of no stage change. As demonstrated Figure 1 (a), one intriguing perception is that not at all like the reaction to 1% hydrogen, which demonstrates monotonic resistance increment with the ingestion of hydrogen, a few moderate stages with lessened rates of resistance increment show up around the expression focuses in the principal cycle of reaction to 2% hydrogen as shown by star checks in Figure 1 (b). These stages flag the event of new stages (α→β). Past specified, the β stage nucleates if the measure of hydrogen consolidation into the interstitial locales of Pd surpasses the strong dissolvability farthest point of hydrogen, and develops with the further retention of hydrogen. Be that as it may, a further increment in hydrogen focus causes serious auxiliary disfigurements and the misshapenings are just mostly recuperated even after hydrogen supply is disengaged as demonstrated the picture in Figure 1 (c).

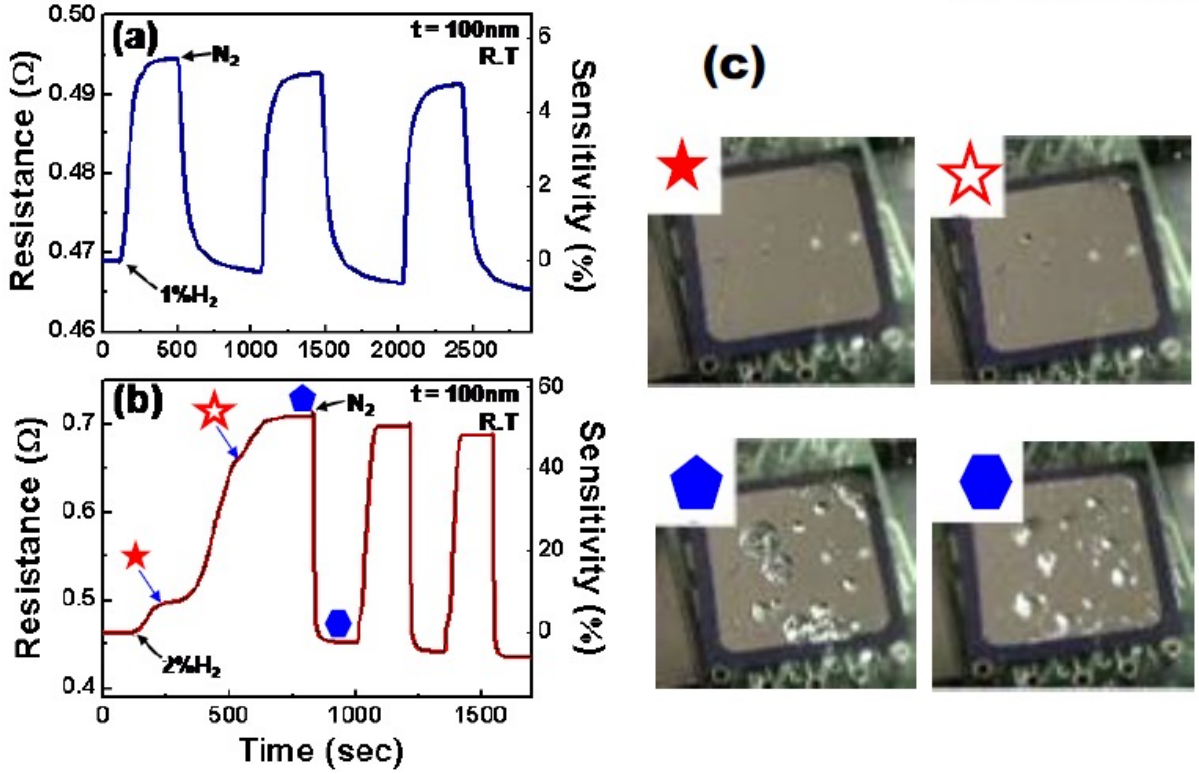

Figure 1. Gas response according to injecting 1% hydrogen and 2% hydrogen with 100 nm thickness of Pd thin film at room temperature (a, b). (c) Film structure deformations are shown according to injection time of 1% hydrogen and morphologies at each steps were indicated by the respective symbols in (b). (a) and (b) Data reproduced from Lee et al. [25] and (c) reproduced from Kim et al. [26].

- **Pd alloy thin film**

The serious auxiliary disfigurements and the non-correspondent hysteretic resistance practices of immaculate Pd films ought to be required arrangements since they chance the unwavering quality and exactness of the Pd film-based hydrogen sensors. Different Pd composites, for example, Pd-Mg, Pd-Au, Pd-Ag, and Pd-Ni have been investigated to keep the auxiliary distortion of the Pd-based thin films [27-29]. Among those, Pd-Au and Pd-Ag combinations have been more concentrated because of their execution points of interest, for example, precious stone structures like that of Pd, higher hydrogen solubilities than immaculate

Pd, and great abilities to stifle auxiliary disfigurements. In any case, they have tricky issues as well. For example, the Au in the Pd-Au amalgam effectively isolates at first glance inferable from its high portability with causing an unwavering quality issue [30]. In addition, on the grounds that the hydrogen separation ability of the compound turns out to be more awful than immaculate Pd, hydrogen gas reaction can be lower.

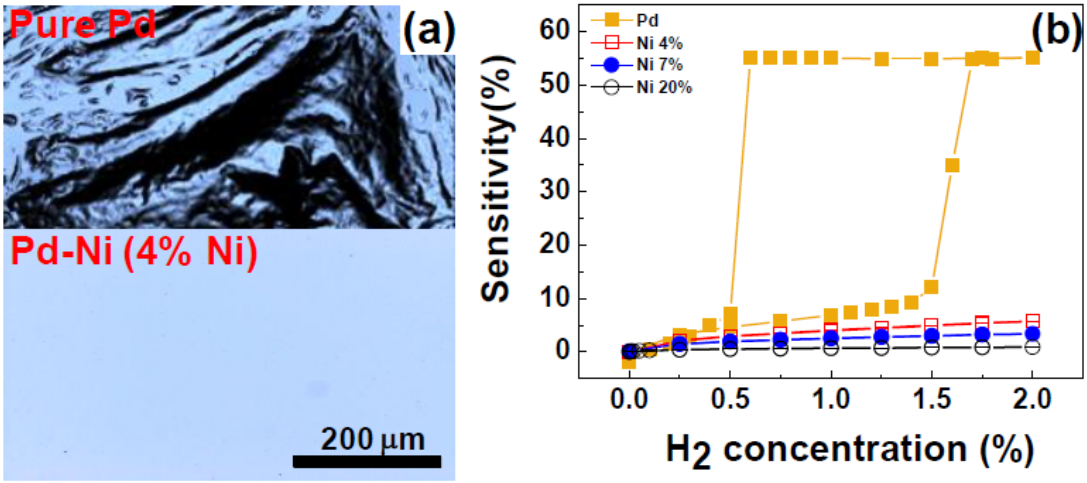

Figure 2. (a) Laser scanning microscopy (LSM) images of a pure Pd and a Pd-Ni alloy (4% Ni) films after exposure to 2% hydrogen. (b) A pure Pd film and Pd-Ni alloy films with changing Ni amount shows gas response and sensitivities according to hydrogen concentration at room temperature. Data reproduced from Lee *et al*. [27].

- **Nanoporous Pd thin film**

Notwithstanding the numerous solid focuses the traditional thick Pd films have as hydrogen sensors, they are for the most part hard to use for measuring hydrogen fixation higher than 500 ppm with exactness. To address these issues, Pd thin films with nanopores have been researched utilizing anodic aluminum oxide (AAO) formats. The AAO-bolstered Pd thin films are relied upon to demonstrate a lower hydrogen location restrict and quicker reaction than the

thick Pd films because of the extraordinarily expanded surface territory. Likewise, the film delamination issue might be eased in the nanoporous structures inferable from the possibly upgraded attachment given by the overwhelming here and there substrate structure. Ding et al. manufactured AAO-upheld nanoporous Pd thin films and contrasted their reaction qualities and those of thick Pd films [28]. To analyze mechanical properties of carbon structure, Young's modulus and hardness of SU-8 structure and pyrolyzed carbon were measured by nanoindentation. As appeared in Figure 23, Young's modulus and hardness of SU-8 were drastically expanded around 5 times and 10 times, each after pyrolysis. Regardless of the possibility that the measured value was much lower than silicon (Table 1), it is bigger than graphite which were utilized as sensor stage material. Strikingly, the thin permeable Pd film could unmistakably recognize hydrogen focus more than 1000 ppm. Taking a gander at the responses of a thick Pd and a permeable Pd films with an undefined thickness of 15 nm, the resistance change in the permeable film was quick and more sensitive than that of the thick Pd film.

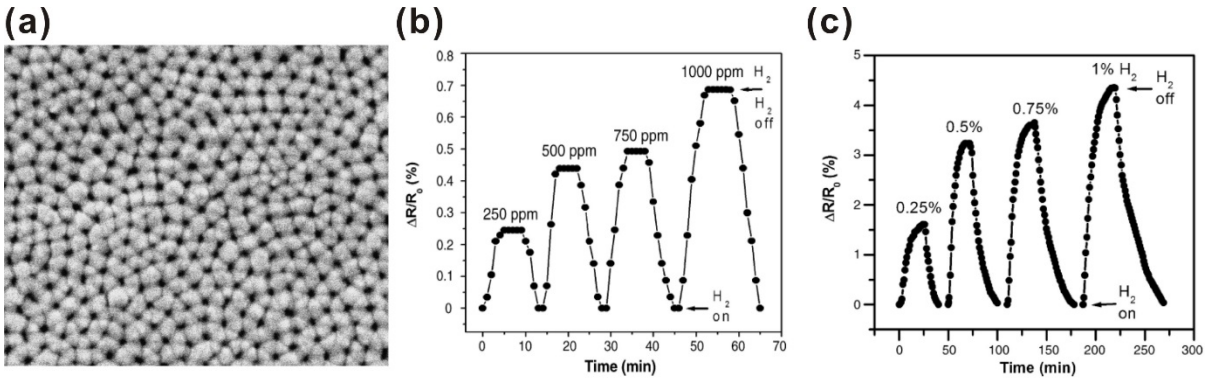

Figure 3. (a) Scanning electron microscope images of nanoporous Pd film fabricated on an

AAO substrate. (b) The relative thin nanoporous Pd film (45 nm) shows gas response and sensitivity at low hydrogen concentration. (c) The relative thick nanoporous Pd film (110 nm) shows gas response and sensitivity at high hydrogen concentration. Data reproduced from Ding *et al*. [28].

- **Pd nanowire**

Through the investigation of nanoporous Pd films portrayed above, it was shown that the hydrogen discovery point of confinement could be enhanced in nanoporous structures because of their expanded surface territory and no structure distortion. On the off chance that it is the genuine case, Pd nanowires would be perfect structures for quick location of wide hydrogen fixations. Be that as it may, the hydrogen detecting properties of the Pd nanowires ought to be considered alongside strategies for their creation, on the grounds that nanowires are when all is said in done harder to manufacture contrasted with thin films and their properties rely on upon the slight auxiliary distinction, for example, width and length.

As Figure 4, lithographically designed Pd nanowires can be viewed as middle of the road structures from Pd thin films and grown Pd nanowires. To fabricate these nanostructures, a blend of E-beam lithography and then a lift-off process was proceeded. To analyze mechanical properties of carbon structure, Young's modulus and hardness of SU-8 structure and pyrolyzed carbon were measured by nanoindentation. As appeared in Figure 23, Young's modulus and hardness of SU-8 were drastically expanded around 5 times and 10 times, each after pyrolysis. Regardless of the possibility that the measured value was much lower than silicon (Table 1), it is bigger than graphite which were utilized as sensor stage material. Hence,

it can be recommended as gas sensor stage in that stiction issue can't be created for outer condition such as gas convection, electrodeposition and joule heating. Pd thin films according to differing thickness t = 20~400 nm were sputter-stored on thermally SiO_2 substrates. The fabricated Pd nanowires had an indistinguishable width w = 300 nm and length l = 10 mm. hydrogen detecting properties of the designed Pd nanowires were examined at room temperature like an element of hydrogen focus and nanowire thickness. The aftereffects of this nanowire are appeared in Figure 5. Figures 5 (a, b) display electrical reactions of two Pd nanowires with t = 20 and 400 nm, separately, at the same hydrogen convergence of 10,000 ppm. The more slender nanowire (t = 20 nm) demonstrates a lower affectability, yet a substantially quicker reaction time contrasted with the thicker one (t = 400 nm). This distinction is credited to the dissemination impact in the more slender nanowire.

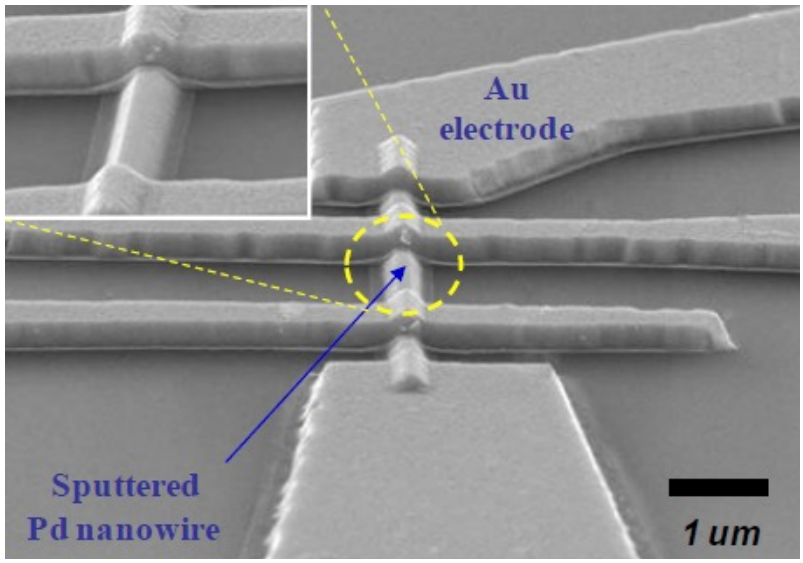

Figure 4. Scanning electron microscope image of palladium nanowire with t = 100 nm, w = 300 nm, and l = 10 mm which is lithographically patterned. Pd nanowire electrodes were patterned with four Ti/Au inner electrodes. Data reproduced from Jeon *et al*. [29].

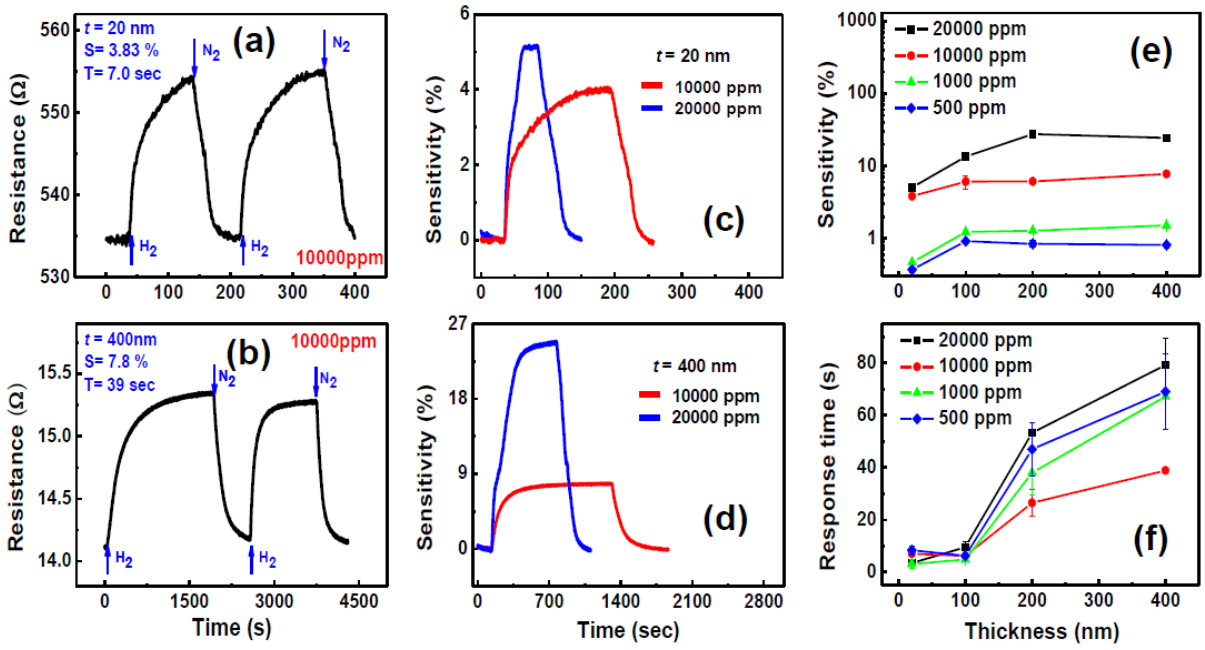

Figure 5. The lithographically patterned Pd nanowires show the gas responses and sensitivity with different thickness **(a)** t = 20 nm and **(b)** t = 400 nm at room temperature when injecting 10000 ppm of hydrogen. Sensitivities of these two types are show upon injecting to 10,000 and 20,000 ppm of hydrogen for the Pd nanowires with different thickness **(c)** t = 20 nm and **(d)** t = 400 nm. **(e)** Gas sensitivity and **(f)** response time are shown as a function of the thickness of Pd nanowires according to hydrogen concentration range of 500 to 20,000 ppm. Jeon *et al*. [29] reproduce these data.

As Figure 6, Pd nanowires which was fabricated by lithography procedures discovered that could be high performed hydrogen sensors with low recognition point of confinement and quick gas reaction. Be that as it may, they perhaps confront the danger of auxiliary distortions at high hydrogen fixations on the grounds that the nanowire post sustained from the substrate. The issue would be explained utilizing base up developed Pd nanowires have no immediate securities with the substrate. That is conceivable to examine more characteristic limited size impacts of hydrogen detecting properties utilizing these Pd nanowires. As a clarification of this base up manufacture, Pd nanowires were developed by electrodeposition process into AAO nanochannel formats by a fluid arrangement with 0.034 mol of $PdCl_2$, utilizing an Au cathode

layer as demonstrated Figure 6(a). Pd nanowires were flushed and inundated in isopropyl liquor (IPA) after artificially evacuating the AAO formats. Figures 6 (b,c) demonstrate agent electrical reactions of two Pd nanowires with d = 20 and 400 nm, separately, at the same hydrogen grouping of 10,000 ppm. On the in spite of lithographically designed nanowires with similar thicknesses, the more slender nanowire (d = 20 nm) displays a bigger affectability than that of the thicker one (d = 400 nm).

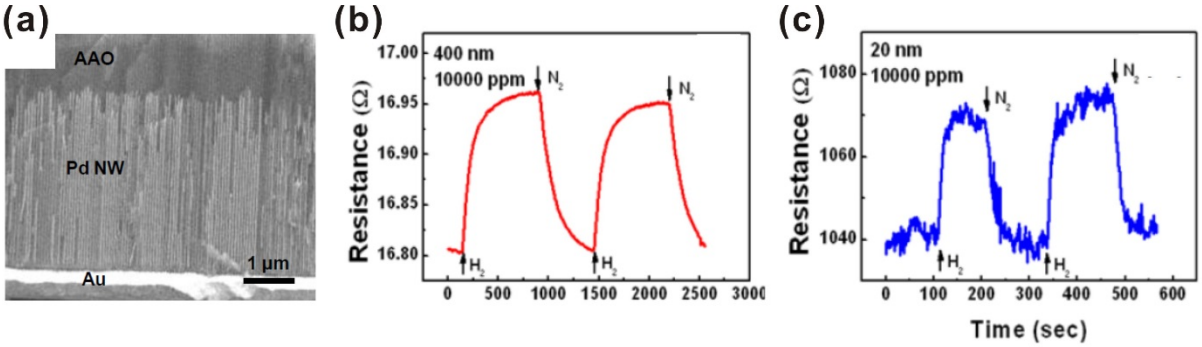

Figure 6. (a) Scanning electron microscope image of electrodeposited multi-Pd nanowires grown into AAO templates with nanochannel. The gas responses of multi-Pd nanowires as a resistance function with different thickness (b) *d* = 400 nm and (c) *d*= 20 nm according to 10000 ppm of hydrogen at room temperature. Jeon *et al*. [30] reproduce these data.

1.2.2 Suspended Pd nanomaterial types

The execution of Pd nanowire depicted above can be constrained by the impacts of the substrates since Pd nanowire ought to be base nanowire by non-firmness and non-strength. These constraints can be overcome by enlivening Pd on suspended nanostructures which are over the substrate at a settled separation. Accordingly, the gas reaction can be improved in light of the fact that a greater amount of the nanomaterial surface zone is presented to the objective gas.

- **Pd thin film coated on the suspended tungsten nanowire**

As demonstrated Figure 7 (a, b) and 8 (a, b), two disconnected microelectrodes with 7 μm hole are associated by flag nanowire connect that measures 10 μm long and 150 nm wide. The nanowire is integrated from the deterioration of tungsten antecedent arrangement by spot lighted Ga+ particles at 30 kV and 12.7 pA particle bar current utilizing financially accessible FIB machine. To upgrade the gas reaction of nanowire to hydrogen, 10 nm thickness of consistently intensified Pd-Pt combination is sputtered on it. After this functionalization, the sputtered Pd-Pt layer turns into a detecting component while the tungsten nanowire stays as a supporting structure.

Figure 8 (c) demonstrates the hydrogen gas reaction to different hydrogen focuses from 1 % to 50 ppm. The greatest resistance change is inside 10 % and the resistance is very much recuperated its unique esteem when the hydrogen gas is cleansed out of the test chamber by 100 % nitrogen gas.

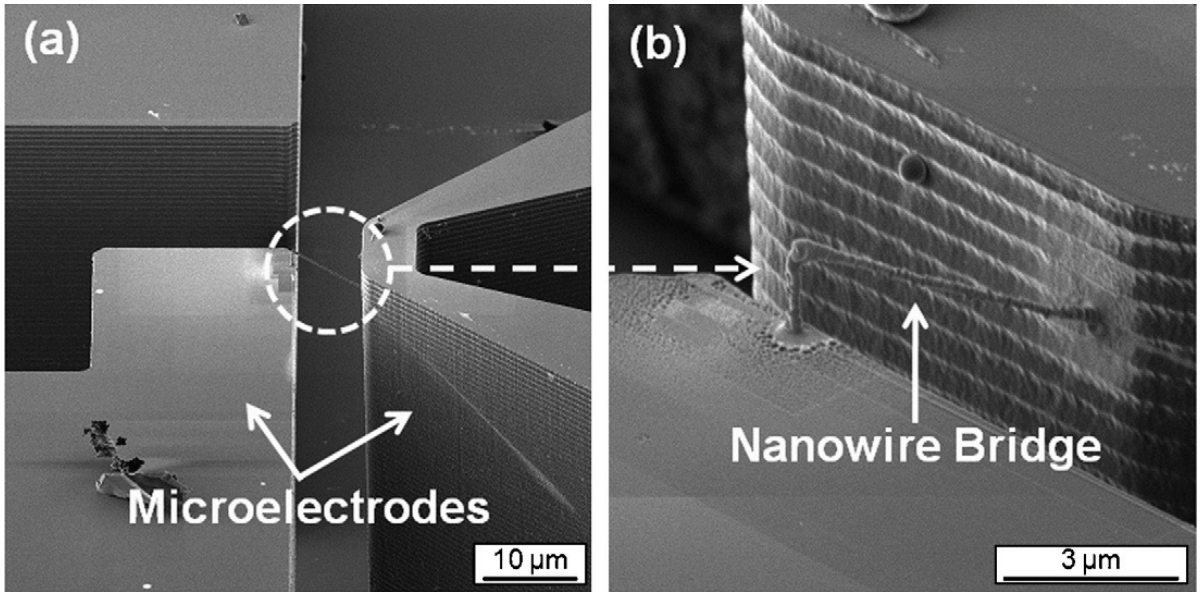

Figure 7. SIM images of nanowire bridge: (a) side view (b) close-up view. Data reproduced from Choi *et al*. [31].

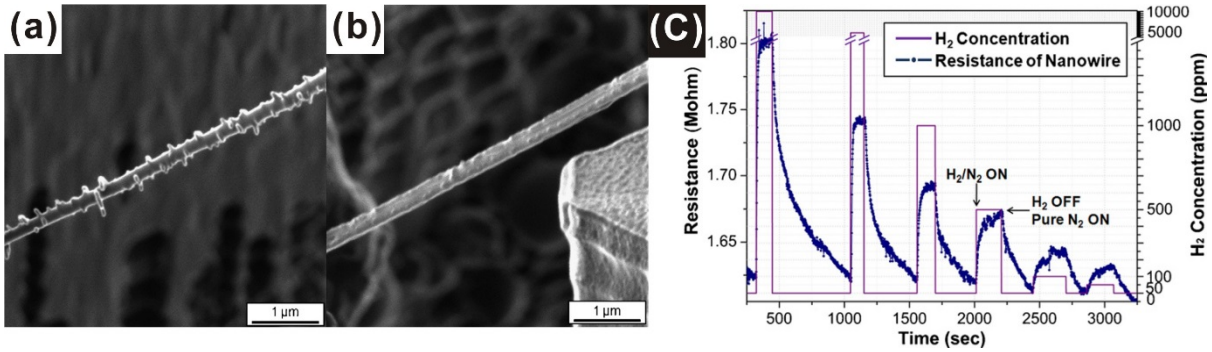

Figure 8. The scanning electron microscope image of surface fabricated tungsten nanowire bridge. (a) The roughness of surface is formed due to FIB-CVD process. (b) The smoothness of surface is due to the Pd–Pt alloy metallization. (c) The resistance and gas response of are shown suspended tungsten nanowire according to different hydrogen concentrations (1% - 50 ppm at room temperature with constant measuring current of 50 nA. Data reproduced from Choi *et al*. [32].

- **Pd thin film coated on the suspended carbon nanowire**

The creation ventures for the carbon nanowire separated from substrate decorated with the Pd layer are shown in Figure 9. Under the carbon terminals, silicon dioxide roof were

designed utilizing isotropic Si carving. These overhang worked as shadow veils amid Pd statement, and in this way, a basic Pd dissipation handle specifically covered the Pd layer (5 nm) just on the suspended carbon nanowire and two carbon cathodes as indicated Figure 10. To upgrade the dominant of the Pd layer on the resistance response of the suspended nanowire, the conductivity of the carbon was changed by controlling the pyrolysis temperature.

Figure 11 demonstrates the consequence of the gas reaction (ΔR/R) estimation of the Pd covered nanowire as differing the hydrogen focus from 500 to 10 ppm and keeping up the temperature of the radiator at 100 ^{o}C on which the hydrogen gas sensor under. The gas reaction expanded relatively to the hydrogen fixation from 10 to 100 ppm and the gas reaction became soaked in light of palladium hydride development.

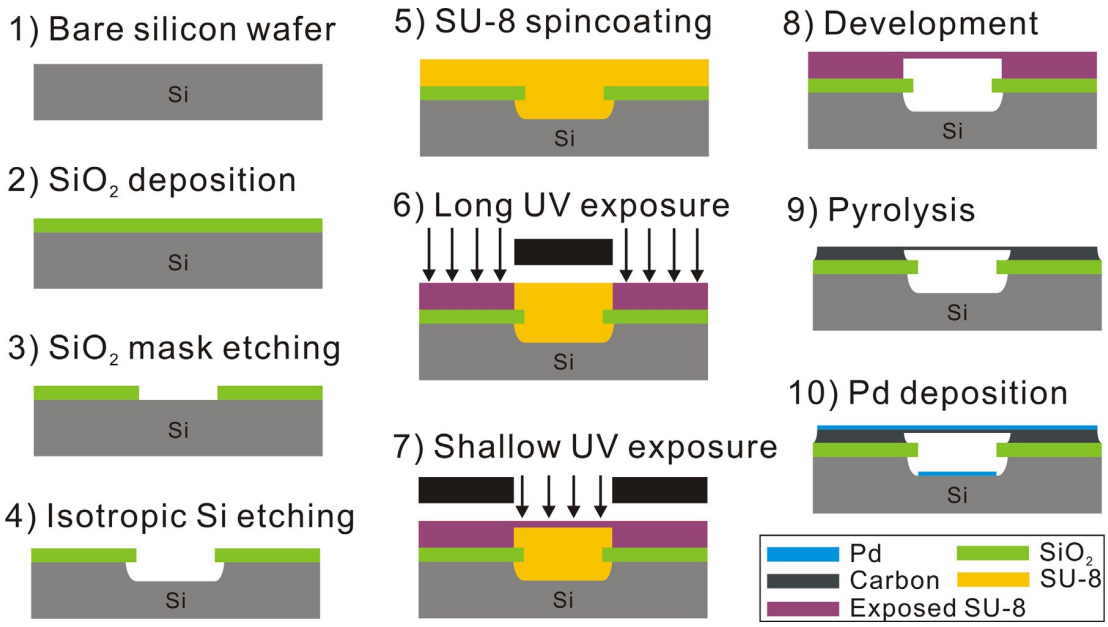

Figure 9. Fabrication steps of suspended Pd thin film coated carbon nanowire. Data reproduced from Lim *et al*. [33]

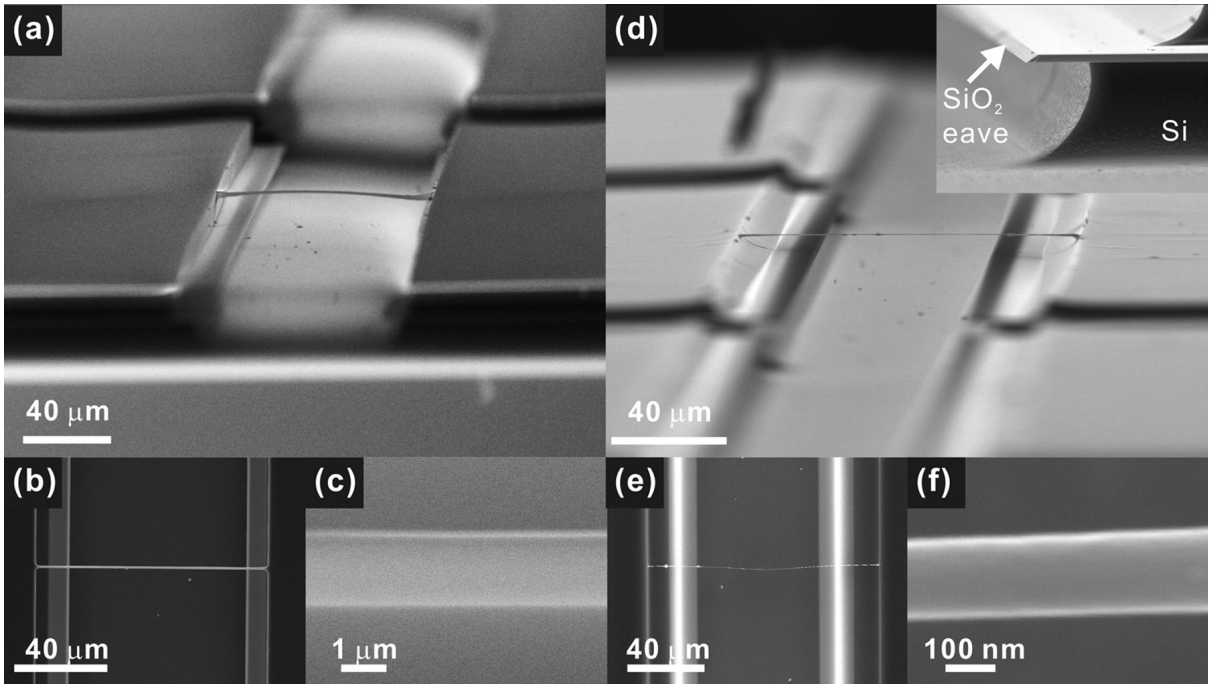

Figure 10. Scanning electron microscope images of a suspended SU-8 polymer microscale wire according to different view angle (a, b, and c). And the pyrolyzed carbon nanowire from polymer microscale wire according to different view angle (d,e, and f). Data reproduced from Lim *et al*. [33]

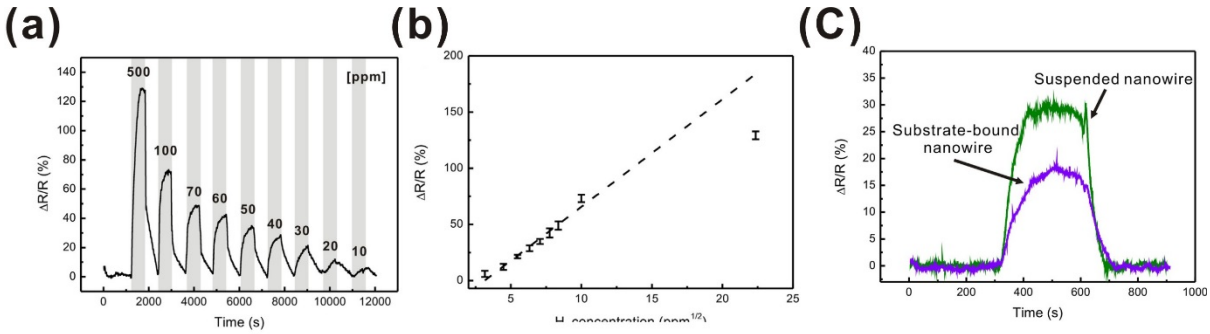

Figure 11. Gas response and sensitivity graph of suspended Pd decorated carbon nanowire. (a) Resistance change graph according to hydrogen concentration (10 to 500 ppm). (b) Sensitivity is shown by gas response vs. square root of hydrogen concentration. (c) Comparing resistnace differences between suspended type and substrate-bound type. Data reproduced from Lim *et al*. [33]

1.3 Self-heating based gas sensor

Conventional gas sensors, including semiconductor oxide sensors and palladium sensors, have been difficult to be integrated into CMOS electronics and wearable electronics due to the relatively high energy consumption by external heater to ensure a rapid and reversible sensing operation via programming the temperature of the sensor between 350 and 670 K. For example, most conventional metal oxide gas sensors can be typically operated at the temperature 670 K by using an external heater. Also, in case of palladium sensor, external heater (350 K) can be often used due to improvement of response and recovery related with sensing performance. The major reason that gas sensors based external heater require relatively high energy consumption is that the external heater must heat up a large volume of sensors via solid heat conduction by competing with the heat dissipation into the surroundings. Thus, thermal management is an important issue for designing sensor electronics.

1.3.1 Metal oxide nanomaterial based sensor

As Figure 12, single crystalline SnO_2 nanowires were consolidated by beat laser statement (PLD) method and vaper-liquid strong (VLS) handle. What's more, from that point onward, SnO_2 nanowire sensor were produced by consistent lithography strategies using electron shaft lithography (EBL) and radiofrequency (RF) sputtering. After contact terminals (Ti/Au layer) declaration and lift-off process, suspended nanowires could be gotten by methods for ousting retribution layer.

To assess the genuine temperature, they gaged the temperature dependence of nanowire resistivity by the 4-test technique with programed outer warmer. Lifting the temperature realizes the decreasing of resistivity, revealing the semiconducting behavior of SnO_2 nanowire. Next, they performed ultrafast current-voltage estimation to probably think the temperature. So

as to gauge the genuine temperature, they quantified the temperature reliance of nanowire resistivity by the 4-test technique with programed outside warmer. Lifting the temperature brings about the diminishing of resistivity, uncovering the semiconducting conduct of SnO_2 nanowire. Next, they performed ultrafast current-voltage estimation to tentatively concentrate the temperature. Therefore, the lifted temperature estimation of the nanowire was evaluated to be ~520 K (13μW) from the temperature reliance information as demonstrated Figure 13.

Figure 14 demonstrates the correlation between various warming strategies including (an) outer warming, (b) self-Joule-warming, and (c) ongoing gas reaction as indicated by NO_2 fixation change, on the resistance change of suspended nanowire gadgets while presenting NO_2 gas (100 ppb). For every single warming structure, exhibiting NO_2 gas extended the resistance of SnO_2 nanowire, as uncovered elsewhere. In outside warmer, growing the temperature from 300 to 520 K on a very basic level redesigned the affectability through propelling the chemisorption on the oxide surface. A similar example on the affectability was in like manner watched while growing the present a motivating force for the self-Joule-warming structure.

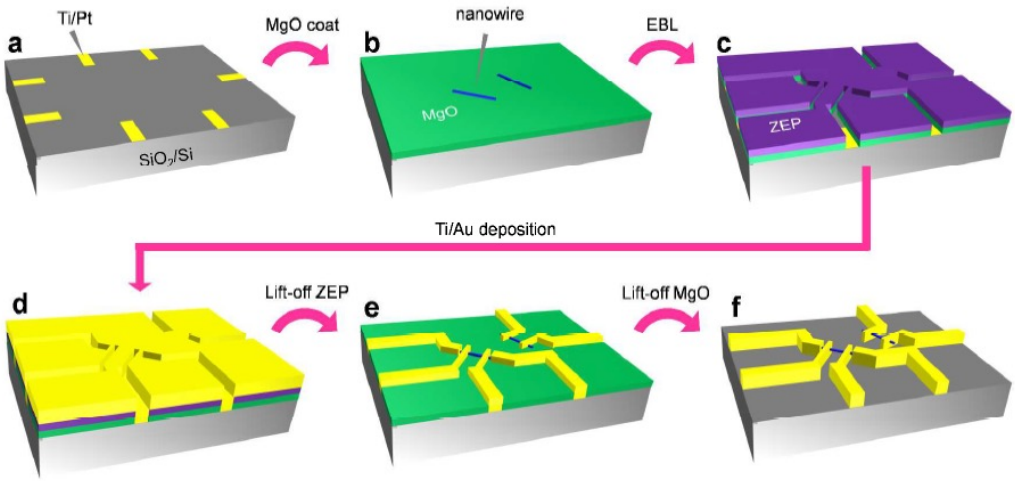

Figure 12. Schematic procedure to fabricate suspended SnO_2 nanowire devices. (a) SiO_2/Si (or PEN) substrate with predefined Ti/Pt electrodes. (b) Depositing MgO sacrificial layer (100 nm) and dispersing SnO_2 nanowires. (c) Spin coating of ZEP resist, EBL drawing, development and etching uncovered MgO layer. (d) Depositing Ti/Au (1nm/300nm) electrode. (e) Lift-off ZEP resist. (f) Dissolving MgO sacrificial layer by dilute HCl solution. Data reproduced from Meng *et al*. [34]

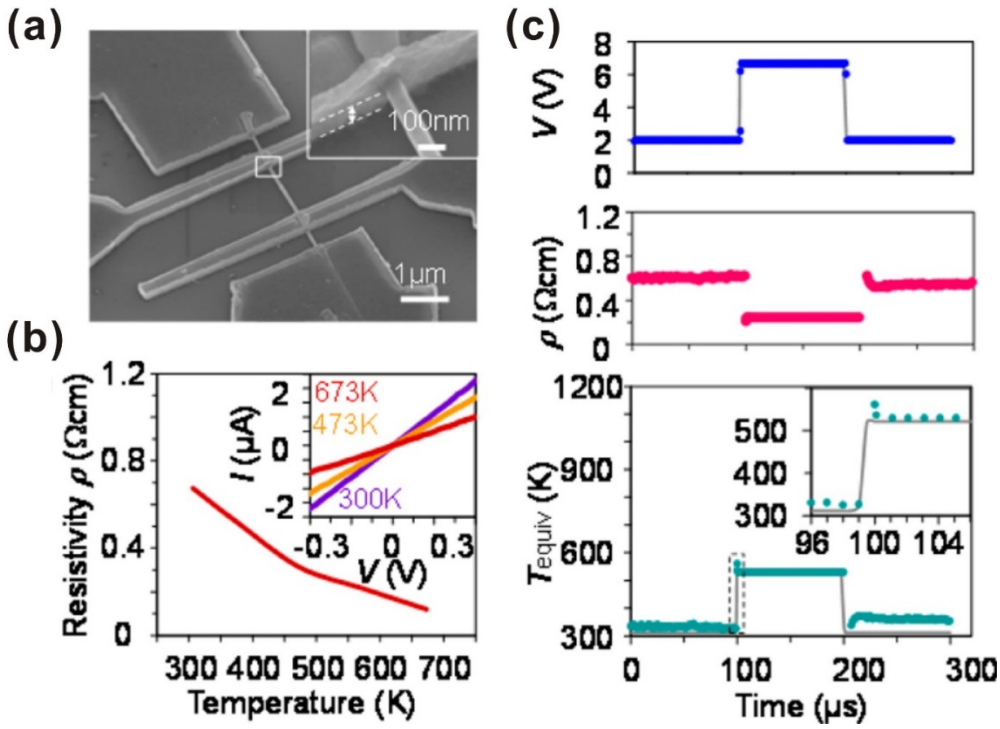

Figure 13. (a) Scanning electron microscope image of 4-gold electrodes which sustained suspended SnO_2 nanowire. (b) Electrical resistivity can be changed according to temperature of this device. The I-V curve is shown for various temperatures in inset graph. (c) Applied voltage, measured conductivity and characterized temperatures graph with real time scale. Gray lines mean simulation results. Data reproduced from Meng *et al*. [34]

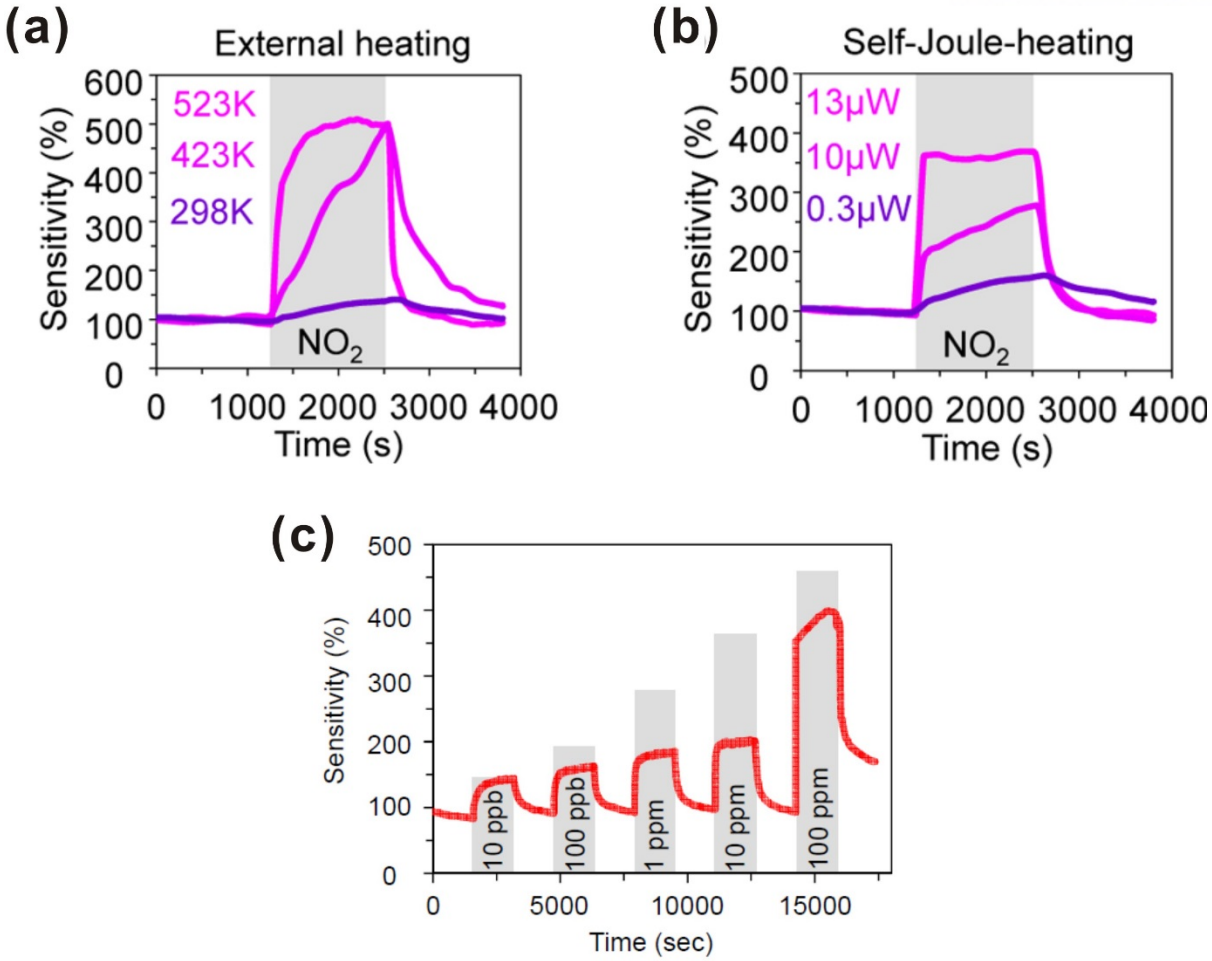

Figure 14. Gas sensing experimental result when injecting NO_2 (100 ppb). (a) Gas response and sensitivity are shown with external heater. (b) Gas response and sensitivity are shown with continuous self-heating. (c) Response of self-heated SnO_2 nanowire to NO_2 with increasing concentration from 10 ppb to 100 ppm. Gradual increase of the sensitivity upon high NO_2 concentrations and steady recovery of device can be found, indicating a good stability. Data reproduced from Meng *et al*. [34]

1.3.2 Pd nanomaterial based sensor

Figure 15 indicates schematic creation of Pd nanoparticle covered Si nanowire. The silicon and silicon dioxide wafer which means silicon layer has a silicon dioxide layer (40 nm) on silicon layer (110 nm). Nanowires (110 nm) were designed by mix of profound bright lithography, responsive particle drawing and photoresist ashing. The nanowire which doped

with n-sort dopants utilizing particle implantation (phosphorus, vitality = 15 keV and measurements = 1 × 1014 cm^{-2}). A silicon nanowire developed silicon oxide (3 nm) utilizing a thermal oxidation process. Framing gas strengthening (10% hydrogen in N_2 surrounding at 400 °C during 30 min) was completed for gadget amongst silicon sample by passivating bonds.

As appeared in Figure 16 (a, b), the gas reaction to a gas injecting 0.5% hydrogen with self-heating was very much coordinated with the gas reaction outside heat condition. Utilizing a similar strategy according to power, we can adjust the temperature as a component of heating force. An exceptionally straight connection of nanowire temperature increment and the power can be appeared in Figure 16 (b).

A short heartbeat (VD = 1.7 V) of Joule warming amid recuperation empowered quick recuperation in Figure 16 (c), a, when contrasted with the no warming condition. Also, the recuperation time was additionally decreased as the beat time expanded,.

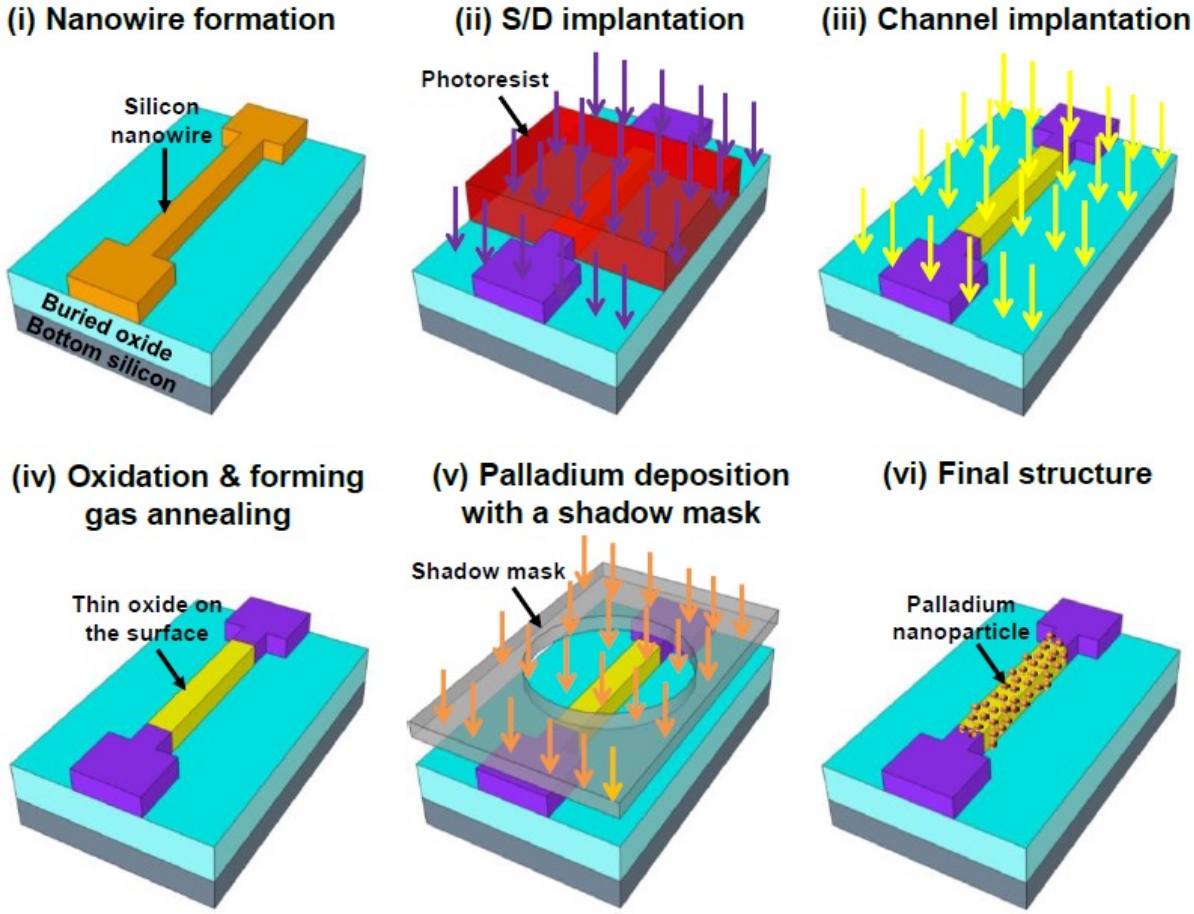

Figure 15. Fabrication of the Pd nanoparticles decorated silicon nanowire gas sensor. Data reproduced from Ahn *et al*. [35]

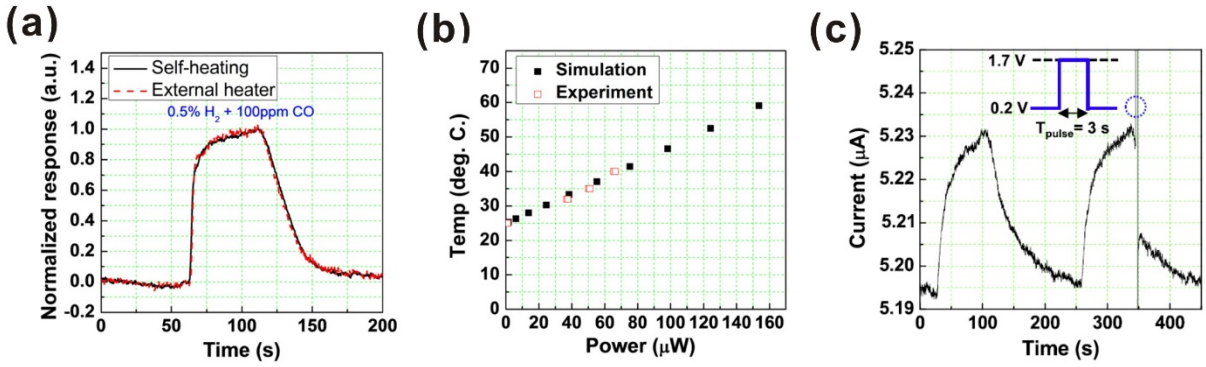

Figure 16. (a) Comparing gas responses between self-heated and external heated silicon nanowire according to injecting 0.5% of hydrogen for the temperature characterization of the self-heating. (b) According to self-heating power, temperature change is shown of the silicon

nanowire. (c) Recovery time improvement with self-heating effect of low power consumption. Data reproduced from Ahn *et al*. [35]

1.4 Novel hydrogen gas sensor based on Pd nanoparticle

In our previous study, we developed a novel hydrogen gas sensor based on an individual, suspended carbon nanowire functionalized with a thin Pd film [33]. Owing to the suspended architecture of the carbon-nanowire template and SiO_2 eaves, a single metal coating process enabled the selective Pd deposition on the carbon nanowire. For structural robustness and high sensitivity, a very thin layer (～5 nm) of Pd was coated on the carbon nanowire. However, this thin Pd layer limited gas absorption, and thus the gas response was saturated even at relatively low hydrogen concentrations(~500 ppm). In addition, although the actual sensor area was at the nanoscale, the whole top surface of the substrate had to be coated with a Pd layer resulting in the material waste. In addition to fast saturation, the Pd film based hydrogen sensor exhibited slow resistance recovery because of the limited diffusion of hydrogen atoms at room temperature. This slow resistance recovery limits precise and continuous detection of fluctuating hydrogen concentrations as shown Figure 17.

In this work, we have overcome two significant limitations of Pd nanostructure based hydrogen sensors: fast gas response saturation or narrow sensing range, and slow resistance recovery. We fabricated arrays of individual carbon nanowires decorated with Pd nanoparticles

using only simple batch microfabrication processes such as carbon-MEMS and electrodeposition. The suspended sensor architecture and large nanoparticle surface area to volume ratio enabled high-sensitivity hydrogen detection with excellent detection limits and fast response times. Furthermore, the PdNP/carbon nanowire based sensor was capable of sensing a wide range of hydrogen concentrations because the Pd nanoparticle size can be controlled by manipulating electrodeposition conditions such as deposition time and potential. For fast and complete resistance recovery, additional current was applied along the PdNP/carbon nanowire to facilitate self-heating. Because of the long, suspended geometry of the PdNP/carbon nanowires, there was very limited heat loss and only 5s of ultra-low-power heating was required for complete and instant resistance recovery as shown Figure 18.

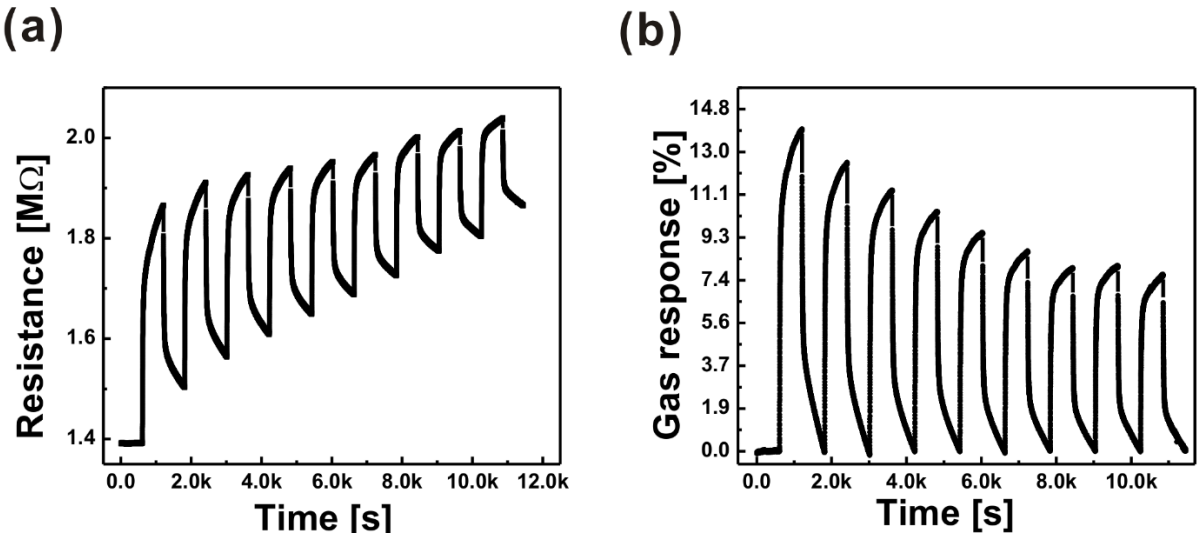

Figure 17. (a) Resistance change of a PdNPs/carbon nanowire in response to hydrogen (100, 90, 80, 70, 60, 50, 40, 30, and 20 ppm in series). (b) Calculated gas response ($\Delta R/R$; ΔR = change in resistance after hydrogen gas injection, R = resistance before hydrogen gas injection) corresponding to the measurement data shown in (a). The gas responses at low concentrations

(40, 30, and 20 ppm) are not differentiated.

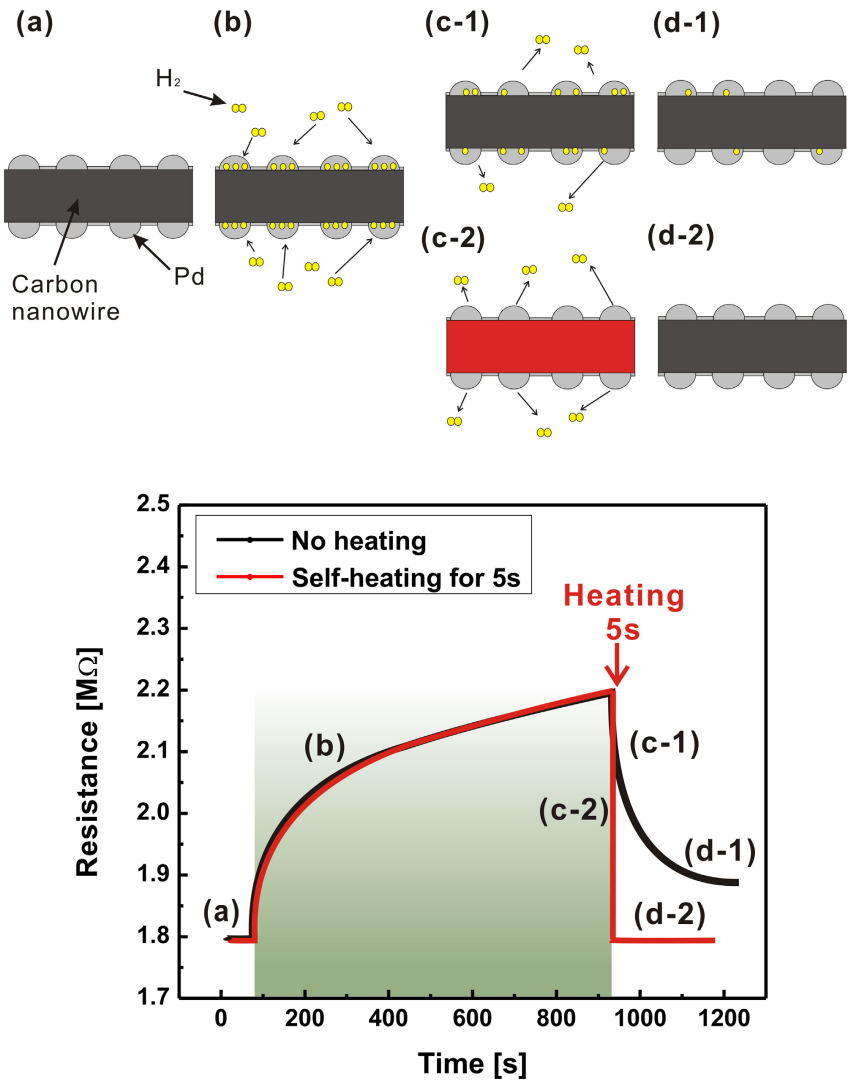

Figure 18. Schematic of the hydrogen gas sensing and self-heating recovery processes of a PdNP/carbon nanowire: (a) Initial state, (b) hydrogen sensing (gas input), (c, d) Recovery (gasremoval); (c-1) no heating (c-2) self-heating, (d-1) slow recovery, (d-2) fast and complete recovery.

1.5 Thesis outline

Here, we introduce details of the sensor fabrication methods, including the carbon-MEMS and electrodeposition process. Carbon-MEMS is a versatile batch microfabrication process which uses UV lithography-based polymer patterning and pyrolysis to create an array of single suspended carbon nanowires decorated with Pd nanoparticles of various sizes. The sensitivity and sensing range can be modulated by controlling the Pd nanoparticle size during electrodeposition. To ensure that the effect of PdNPs on the composite nanowire resistance dominates and produces a large hydrogen gas response, the resistivity of the carbon nanowire was modulated by controlling the pyrolysis temperature. In addition, reproducible hydrogen gas sensing capabilities driven by fast, complete gas response recovery are demonstrated.

2 Experimental

2.1 Overview of PdNP/carbon nanowire hydrogen gas sensor fabrication

In this research, as shown Figure 19, an array of suspended carbon nanowires were fabricated using carbon-MEMS process of UV-lithography and pyrolysis. Polymer microwires patterned by UV-lithography were converted into nano-sized carbon nanowires due to isotropic volume reduction via pyrolysis. On separate carbon nanowires, Pd nanoparticles were selectively integrated with different electrodeposition conditions as shown in Figure 2 (NW1: 0.8 V for 5 s after 1.2 V for 5 s; NW2: 0.8V for 25 s after 1.2 V for 5 s). Owing to relatively high resistance of carbon nanowires, Pd NPs work as the bypass of electrical current flow. As a result, the resistance of a Pd/carbon nanowire changes depending on hydrogen concentration. Besides, temperature of Pd/carbon nanowire can be instantaneously increased with ultra-low-power (30 μW) Joule heating owing to the suspended nano-structure. As a result, slow recovery problem frequently found in chemiresistor-based gas sensors can be overcome.

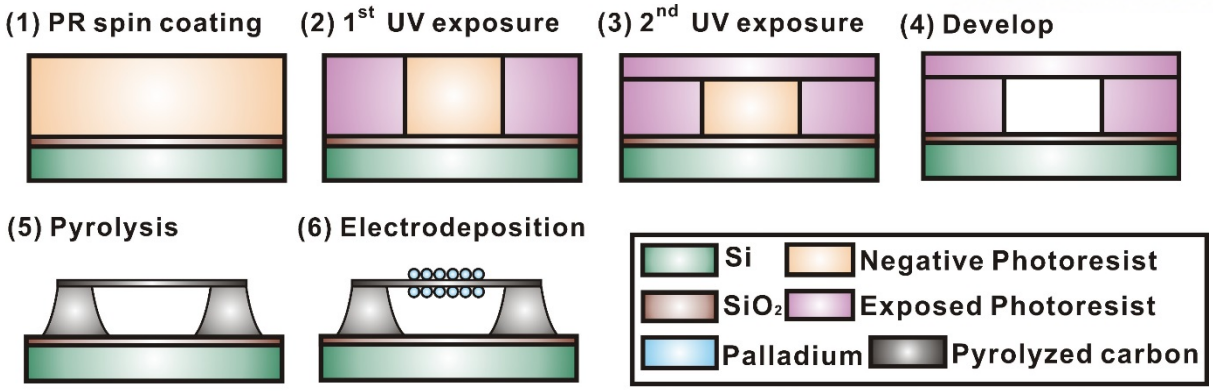

Figure 19. Schematic of the fabrication of a suspended carbon nanowire coated PdNPs.

2.2 Suspended carbon nanowire – Carbon-MEMS

The fabrication steps used to make the suspended carbon nanowire functionalized with Pd nanoparticles are illustrated in Figure 19, 1μm-thick SiO_2 insulation layer was grown on a 6-inch Si wafer (p-type, boron doped, 5 – 20 Ωcm, thickness = 660 – 700 μm; LG Siltron Co., Ltd., Korea) via wet oxidation. Polymer precursor structures including suspended microwires were patterned using two successive UV lithography processes. For the patterning of polymer posts that supported the suspended microwires, a spin-coated 20 μm-thick negative photoresist layer (SU-8 2025, Microchem. Corp., USA) was exposed from top to bottom. Upon the second UV exposure, suspended polymer microwires were polymerized just at the shallow top polymer area with a low dose. After a post-exposure bake step, the solid polymer structure, including suspended wires and their supporting posts, was characterized in a solitary advancement handle. The solid polymer forerunner structures were changed over into solid carbon structures by means of pyrolysis in vacuum. Amid pyrolysis, the photoresist structures

shrank significantly. Subsequently, the widths of the suspended polymer wires diminished to nanometer scale while the suspended structures wound up noticeably stretched in light of volume decrease in the post structures.

2.3 Pd nanoparticles decorated carbon nanowire – Electrodeposition

Pd nanoparticles were grown on the suspended carbon nanowires via electrodeposition in a 1 mM Pd electrolyte solution, Na_2PdCl_4 (98% purity, Sigma Aldrich Co., USA). During electrodeposition, the monolithic carbon structure was biased with various potentials (-0.6 − -1.5 V vs the Ag/AgCl pseudo-reference electrode) and a platinum wire was used as the counter electrode. After electrodeposition, the sensor chip was annealed at 100 ^{o}C in vacuum (1.0×10^{-5} Torr) for 20 min using a rapid thermal process (KVR6000, Korea Vacuum Tech. Ltd., Korea).

2.4 Experimental setup

The change in the electrical resistance of the suspended PdNP/carbon nanowire in response to hydrogen was measured at atmospheric pressure and room temperature in a gas chamber equipped with mass flow meters as illustrated in Fig. S3. Due to the limited flow rates of mass flow controllers and the laboratory safety rule, the hydrogen gas detection was performed for 10 ppm – 5 % of hydrogen. Before hydrogen gas detection, the chamber was purged via several vacuum and N_2 purge cycles. Hydrogen concentrations were controlled by mixing 5 % hydrogen in air with pure air using a gas flow controller (GMC1200, Atovac,

Korea). While the hydrogen/air gas mixture flowed through the gas chamber at room temperature, electrical current was applied through two carbon posts and the voltage drop along the PdNP/carbon nanowire was measured using a source meter (Keithley 2401, Keithley Instruments, Inc., USA). The input power was set to ~ 6.25 nW during the gas concentration measurement and then, increased to ~ 30 μW for 5 s when the hydrogen gas was closed resulting in fast and complete recovery.

The morphologies of suspended PdNP/carbon nanowires were characterized via Scanning electron microscope (Quanta 200, FEI Company, USA). The microstructures and crystallinities of Pd nanoparticles coated on a suspended carbon nanowire were characterized via HRTEM (JEM-2100F, JEOL Ltd., Japan). The TEM sample was prepared using a focused-ion-beam (FIB) milling machine (Helios 450HP, FEI company, USA). To reduce Ga ion-induced damage to the Pd nanoparticles, an extra Pd layer was electrodeposited.

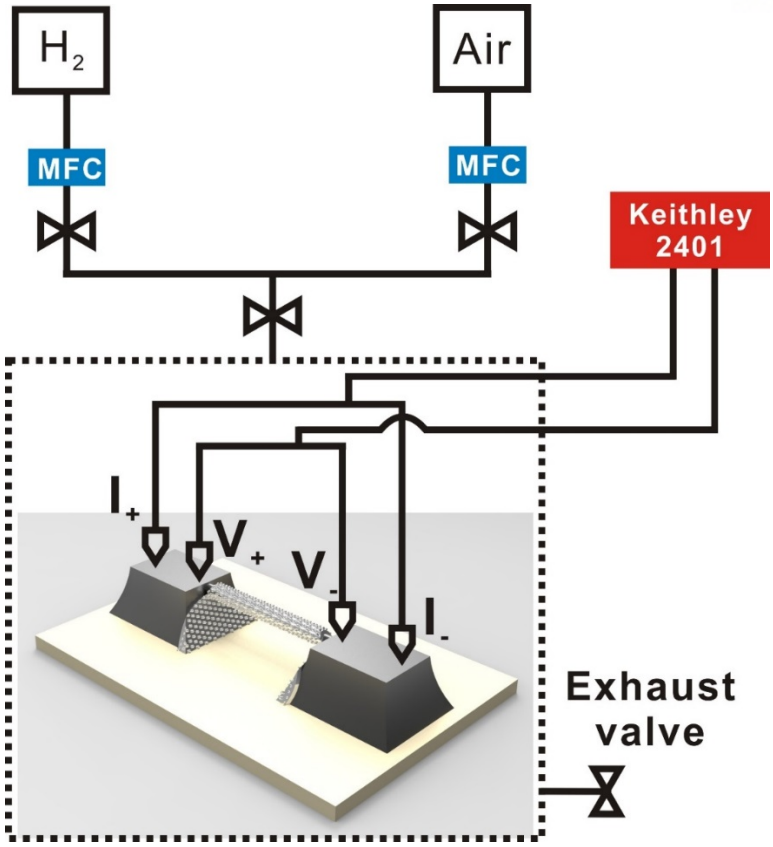

Figure 20. Scanning electron microscope (Scanning electron microscope) images of (a, b) monolithic SU-8 structure and (c, d) monolithic mixed-scale convex carbon mold. (b) Two different scale polymer precursors are vertically connected

3 Results

3.1 Morphologies of PdNP

3.1.1 Pyrolyzed suspended carbon nanowire

The fabrication steps used to make the suspended carbon nanowire functionalized with Pd nanoparticles are illustrated in Figure 21. A 1 μm-thick SiO2 insulation layer is grown on a 6-inch Si wafer (p-type, boron doped, 5 – 20 Ω cm, thickness = 660 – 700 μm; LG Siltron Co., Ltd., Korea) via wet oxidation. Polymer precursor structures including suspended microwires are patterned using two successive UV lithography processes. For the patterning of polymer posts that support the suspended microwires, a spin-coated 20 μm-thick negative photoresist layer (SU-8 2025, Microchem. Corp., USA) is exposed from top to bottom. Upon the second UV exposure, suspended polymer microwires is polymerized only at the shallow top polymer region with a low dose. After a post-exposure bake step, the monolithic polymer structure, including suspended wires and their supporting posts, is defined in a single development process. The monolithic polymer precursor structures are converted into monolithic carbon structures via pyrolysis in vacuum. During pyrolysis, the photoresist structures shrink dramatically. Thus, the diameters of the suspended polymer wires decrease to nanometer scale while the suspended structures became elongated because of volume reduction in the post structures. Finally, Pd nanoparticles are grown on the suspended carbon nanowires via electrodeposition in a 1 mM Pd electrolyte solution, Na_2PdCl_4 (Aldrich, 98% purity).

During electrodeposition, the monolithic carbon structure is biased with various potentials (-0.6 − -1.5 V vs the Ag/AgCl pseudo-reference electrode) and a platinum wire is used as the counter electrode. After electrodeposition, the sensor chip is annealed at 100 ^{o}C in vacuum (1.0 × 10−5 Torr) for 20 min using a rapid thermal process (KVR6000, Korea Vacuum Tech. Ltd., Korea).

The change in the electrical resistance of the suspended PdNP/carbon nanowire in response to hydrogen was measured at atmospheric pressure and room temperature in a gas chamber equipped with mass flow meters. Before hydrogen gas detection, the chamber was purged via several vacuum and N2 purge cycles. Hydrogen concentrations were controlled by mixing 5 % hydrogen in air with pure air using a gas flow controller (GMC1200, Atovac, Korea). While the hydrogen/air gas mixture flowed through the gas chamber at room temperature, the change in the electrical resistance of the PdNP/carbon nanowire was measured using a source meter (Keithley 2401, Keithley Instruments, Inc., USA).

The morphologies of suspended PdNP/carbon nanowires were characterized via Scanning electron microscope (Quanta 200, FEI Company, USA). The microstructures and crystallinities of Pd nanoparticles coated on a suspended carbon nanowire were characterized via HRTEM (JEM-2100F, JEOL Ltd., Japan). The TEM sample was prepared using a focused-ion-beam (FIB) milling machine (Helios 450HP, FEI company, USA). To reduce Ga ion-induced damage to the Pd nanoparticles, an extra Pd layer was electrodeposited.

To analyze mechanical properties of carbon structure, Young's modulus and hardness of SU-8 structure and pyrolyzed carbon were measured by nanoindentation. As appeared in Figure 23, Young's modulus and hardness of SU-8 were drastically expanded around 5 times and 10 times, each after pyrolysis. Regardless of the possibility that the measured value was much lower than silicon (Table 1), it is bigger than graphite which were utilized as sensor stage material. Hence, it can be recommended as gas sensor stage in that stiction issue can't be created for outer condition such as gas convection, electrodeposition and joule heating.

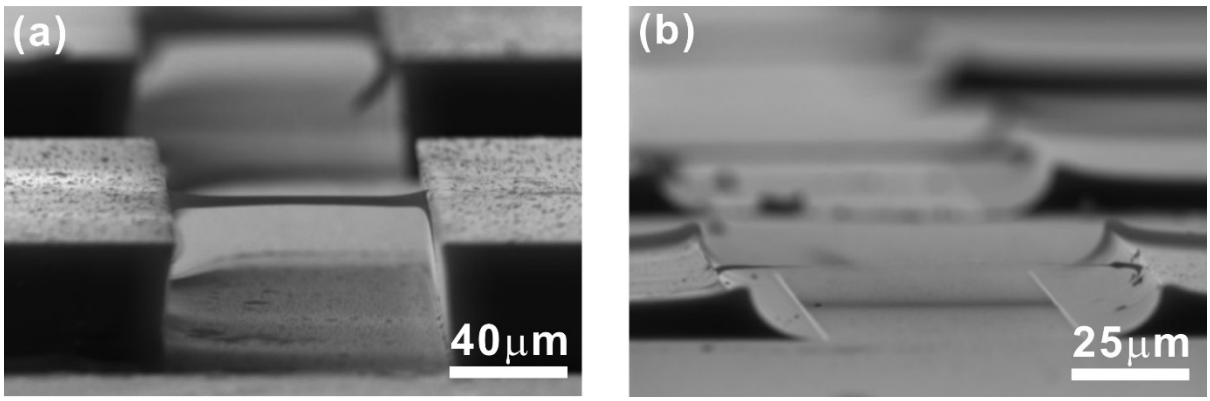

Figure 21. Scanning electron microscope images of bridge-shaped polymer before pyrolysis (a) and carbon nanowires after pyrolysis (b) with bent supports corresponding to the polymer suspended microwires.

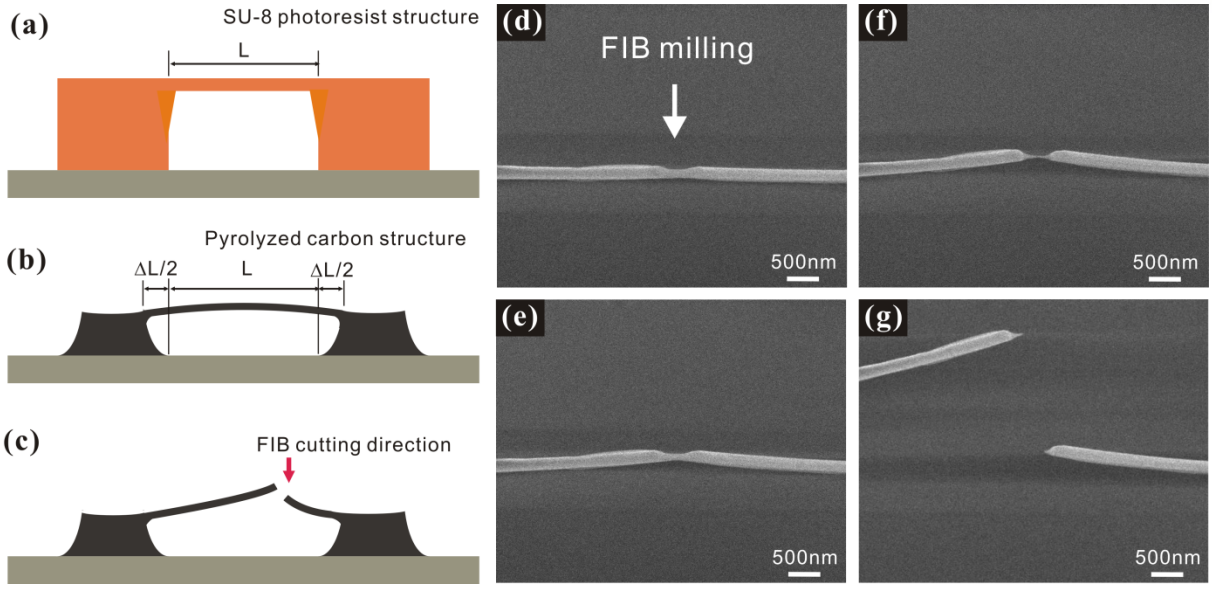

Figure 22. Schematic diagrams of (a) a SU-8 photoresist structure before pyrolysis and (b) a corresponding pyrolyzed carbon structure, (b) schematic diagram of a FIB processed suspended carbon nanowire, and (d)-(g) Scanning electron microscope images of a single suspended carbon nanowire as a FIB milling process proceeds. Data reproduced from Ahn *et al*. [36]

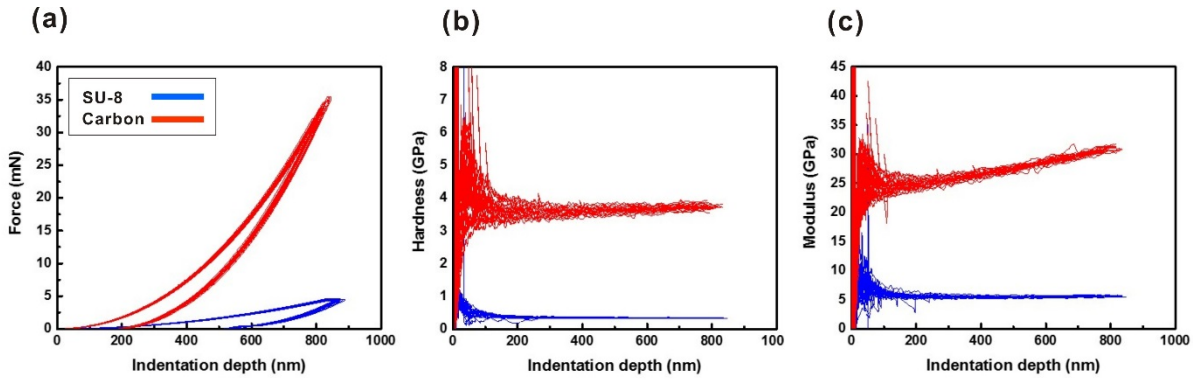

Figure 23. Nanoindentation measurements of SU-8 structures and pyrolyzed carbon. (a) input force for measuring, (b) Hardness of SU-8 and pyrolyzed carbon and (c) Modulus of SU-8 and pyrolyzed carbon.

	SU-8 (measurement)	Carbon (measurement)	Silicon (reference - wiki)	Graphite
Young's modulus(GPa)	5.5±0.1	28.8±0.4	130 - 188	8-15
Hardness (GPa)	0.35±0.01	3.67±0.07	10.2	0.3

Table 1. Nanoindentation measurements of SU-8 structures and pyrolyzed carbon. After pyrolysis, modulus and hardness were dramatically increased. Comparing with silicon, Young's modulus and hardness is small, but it is larger than graphite which is enough to be used sensor platform.

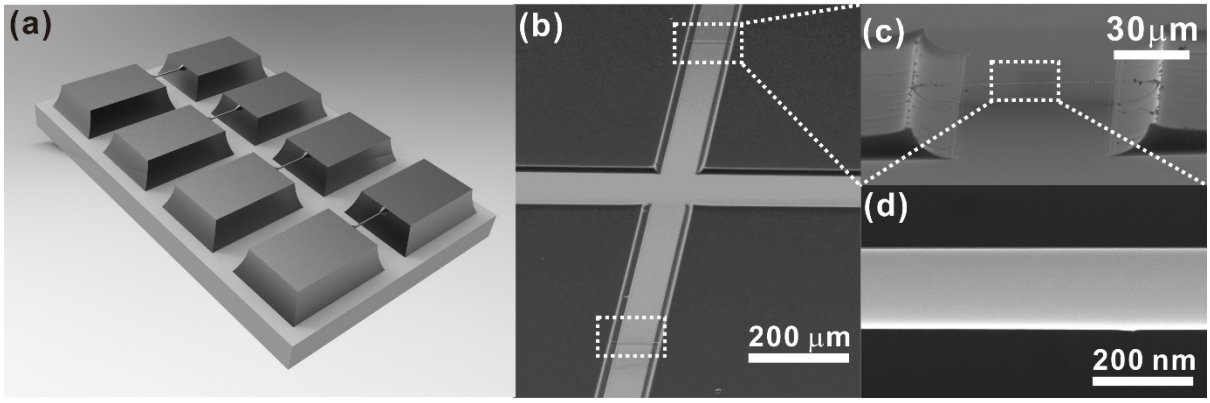

Figure 24. (a, b) Schematic and Scanning electron microscope images of an array of two different types of single suspended carbon nanowires integrated onto a single chip. (c) Bird's-eye view, (d) enlarged views Scanning electron microscope images of carbon nanowire.

3.1.2 Pd nanoparticles decorated carbon nanowire

To understand the effects of electrodeposition parameters such as potential and deposition time, systematic deposition of Pd nanoparticles was performed. First, the effect of electrical potential on the nanoparticle morphology was characterized by applying various levels of potential (−0.4, −0.8, and −1.2 V vs Ag/AgCl) to suspended carbon nanowires (diameter ~200 nm, length ~100 μm)for 5 s. The number of Pd nucleation sites increased

with the applied potential, and thus the carbon nanowire became uniformly coated with Pd seed particles at −1.2 V, as shown Fig. S4. After the nucleation step (−1.2 V for 5 s), the nanoparticle size was controlled by manipulating the electrodeposition time. For nanoparticle size control, the electrodeposition step used a lower potential (−0.8 V vs Ag/AgCl) than the nucleation step. In this study, two different sizes of PdNPs were deposited on suspended carbon nanowires. The growth conditions of the composite wires were varied and the samples were named NW1 and NW2 (NW1: −1.2 V for 5 s and−0.8 V for 5 s, NW2: −1.2 V for 5 s and −0.8 V for 25 s). The sizes of the Pd nanoparticles increased with the growth step deposition time. Thus, uniform coating with two different sizes of PdNPs occurred, as shown in Figure 27. In this research, the hydrogen gas sensing performances of these two types of suspended PdNP/carbonnanowires were characterized.

The crystallinities and microstructures of PdNPs grown on suspended carbon nanowires were characterized via HR-TEM as shown in Fig. S5. We prepared PdNPs larger than those used inNW1 and NW2 (~70 nm) because small PdNPs are easily damaged during FIB sample preparation. The TEM image and well-defined fringe patterns indicate that the PdNPs are highly crystallized (Figure 26). The interplanar spacings of the Pd lattice fringes are 0.23 and 0.2 nm, which correspond to the (111) and (200) lattice planes, respectively, of the face-centered cubic (fcc) Pd structure. And it was shown that these crystallinities were related with

high hydrogen absorption and sensing performance.

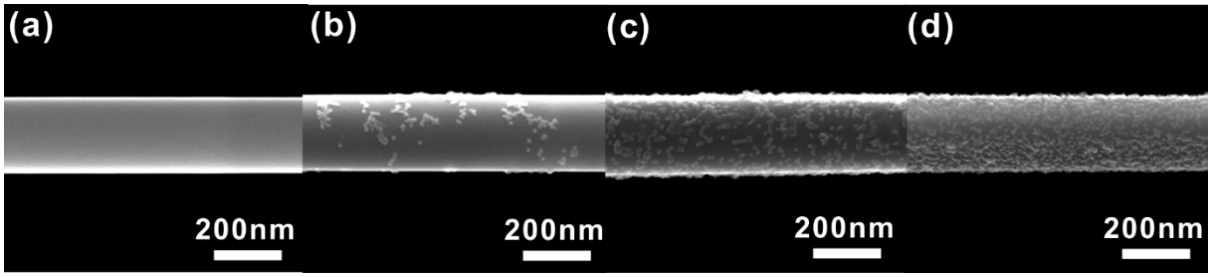

Figure 25. Scanning electron microscope images of (a) a bare carbon nanowire and (b, c, d) carbon nanowires decorated with PdNPs with various potentials applied: (b) -0.4 V for 5 s, (c) -0.8 V for 5 s, and (d) -1.2 V vs the Ag/AgCl pseudo-reference electrode in 1 mM Na_2PdCl_4 for 5 s.

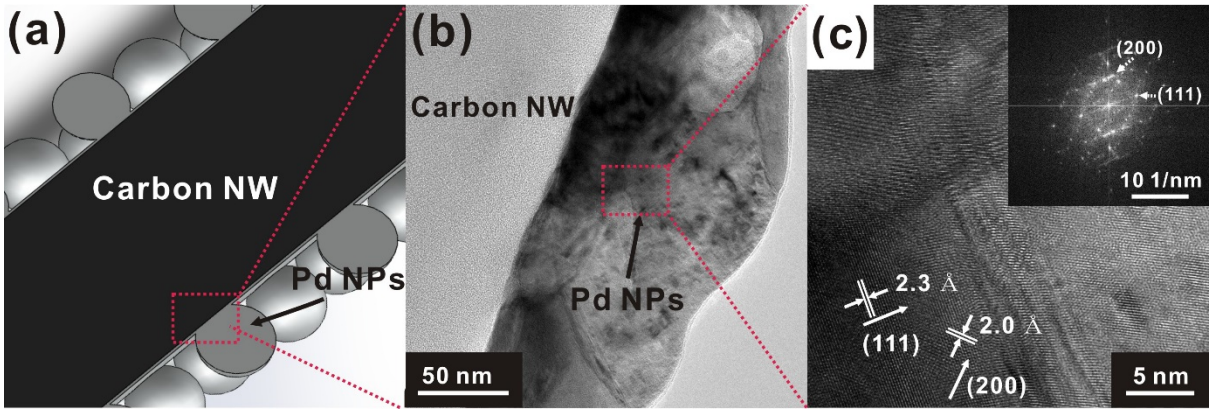

Figure 26. (a, b) Schematic and TEM images of individual, suspended PdNP/carbon nanowires. (c) Magnified HRTEM image and diffraction pattern (inset image) of PdNPs.

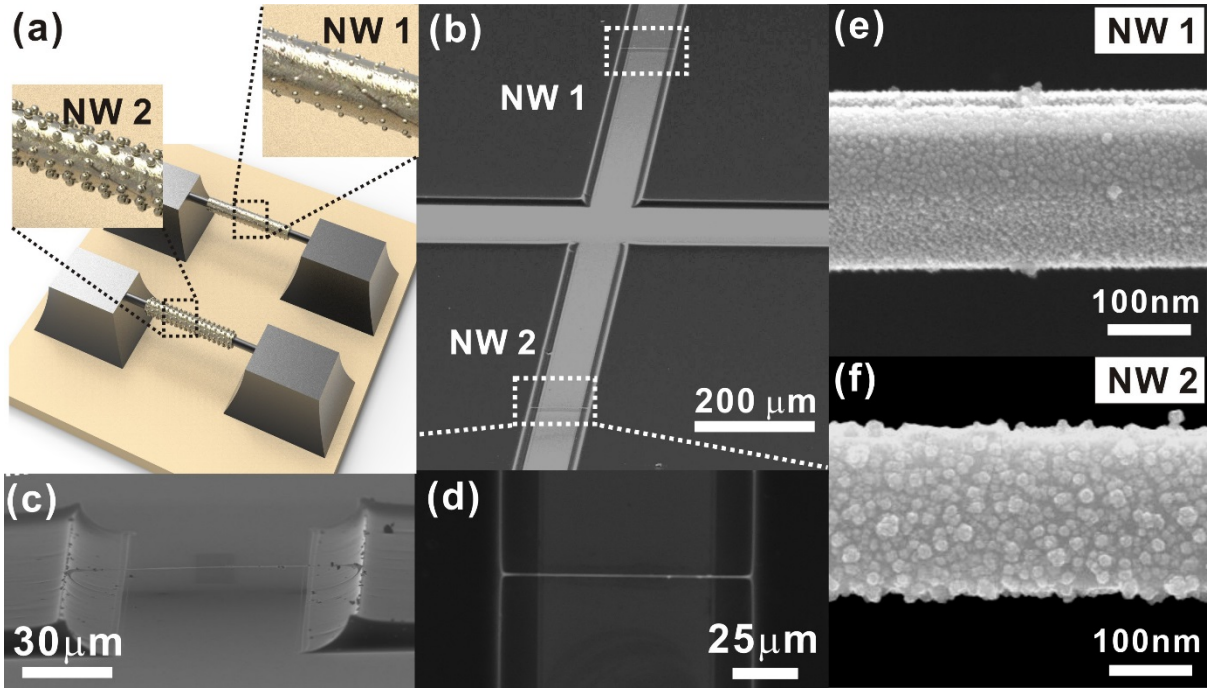

Figure 27. (a, b) Schematic and Scanning electron microscope images of an array of two different types of single suspended PdNP/carbon nanowires integrated onto a single chip. (c) Bird's-eye view, (d) top view, and enlarged views of (e) small PdNPs (NW1) and (f) large PdNPs (NW2).

3.2 Characterization of the electrical properties of PdNP/carbon nanowire

3.2.1 Current bypass through PdNP on carbon nanowire

Through measuring the electrical resistance change of the Pd coated carbon nanowire, hydrogen gas sensing was possible. The electrical resistance is characterized by the resistance of the carbon core and the electrodeposited Pd nanoparticles layer along nanowire. We can thick that the suspended carbon wire and the coated Pd nanoparticles layer are separated like parallel electrical circuit with the distance difference between the carbon pillars and the suspended nanowire. Therefore, the electrical resistance was more sensitive to the hydroge

injected resistance of the Pd coated nanowire changing of the Pd nanoparticles layer according to hydrogen concentration change as the ratio of the resistance of the carbon nanowire to that of the Pd nanoparticles layer increases. And then, the experiment is proceeded which is measuring resistance of nanowire according to increasing temperature of oven because the resistance of nanowire can be increased according to increasing temperature as shown Figure 30 (a). Figure 34 (a) shows schematic image about sample modeling of which the resistance can be measured in oven. Next, the resistance was measured at two environments such as N_2 and Air. But, two environments cannot generate difference because Pd nanomaterial. After electrodeposition of Pd nanoparticles layer, total resistance of Pd coated nanowire can be decreased due to current bypass into Pd nanoparticles layer. These results can be demonstrated with COMSOL Multiphysics simulation (Figure 29. (b)), metal-type conductivity-temperature relationships and I-V curve conductivity measurement as shown Figure 30. (a, b). The gas response is continuously increased at 6.25 nW applied power when 1000 ppm hydrogen injected as shown Figure 39 black line. In this case, exact hydrogen concentration calibration can be impossible at real sensing environment due to changeable gas response. However, this problem can be solved by continuous self-heating not spontaneous self-heating (5s). As shown Figur 39, green line show saturation phenomenon with low gas response and pink line show quickly saturated gas response (< 5s) due to low gas solubility and fast kinetic hydrogen molecules. First, electrodeposition of PdNPs reduced the electrical resistance of the suspended

composite nanowires by 3.5 and 15 times for NW1 and NW2, respectively. Both of the composite nanowires exhibited good Ohmic contact, as shown Figure. 3(b).

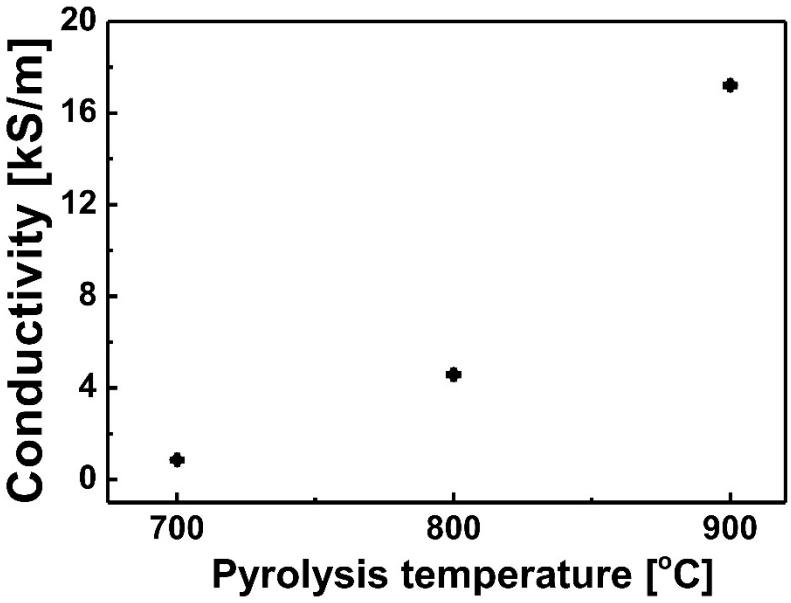

Figure 28. Change of electrical conductivities according to pyrolysis temperature (700, 800 and 900°C) at room temperature.

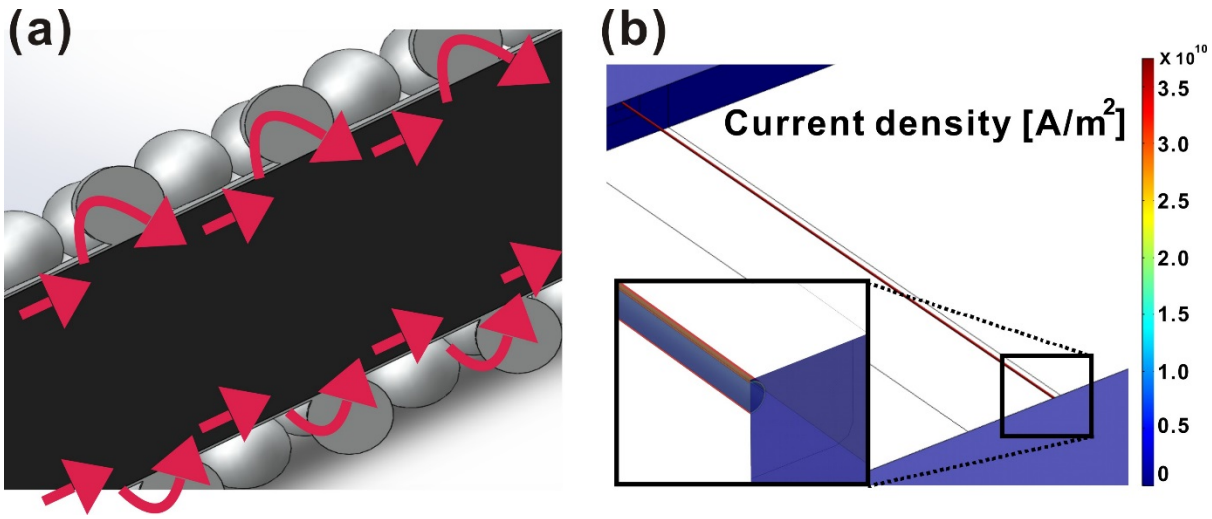

Figure 29. (a) Schematic image about principle of electrical current bypass on PdNP/carbon nanowire. (b) Simulation result for current density of PdNP/carbon nanowire demonstrating current bypass into Pd nanoparticles.

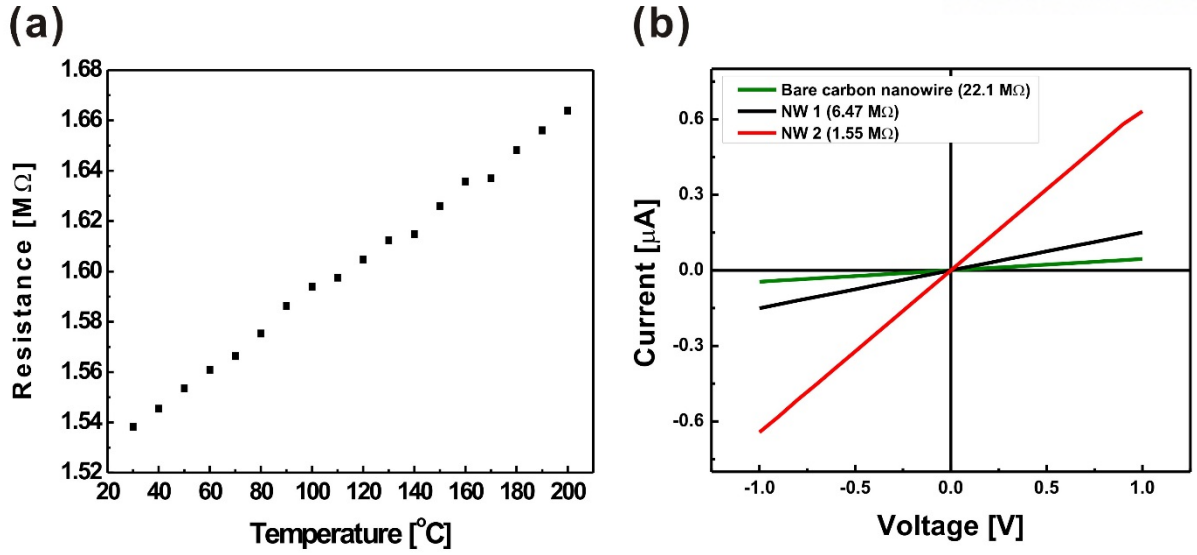

Figure 30. (a) PdNP/carbon nanowire conductivity-temperature relationships. (b) I-V characteristics of a suspended carbon nanowire before and after Pd nanoparticle deposition.

3.3 Characterization of the thermal properties of PdNP/carbon nanowire

3.3.1 Hydrogen sensing performance according to self-heating

As previously mentioned, Joule-heat-based self-heating was used to enhance kinetic interactions between gas molecules and the sensor surface. In no heating case, it takes over 3 hour in order to recover initial resistance value (1.55 MΩ). However, in self-heating case, the increase in resistance caused by gas absorption could be recovered instantaneously. Because of the sub-micrometer diameter of the suspended PdNP/carbon nanowire, and because the delicate nanowire is detached from the substrate, measurement of changes in the temperatures of the suspended nanowires is limited. Instead, the effect of the self-heating was evaluated by comparing the resistance recovery rates of a suspended PdNPs/carbon nanowire under various heating scenarios, as shown in Fig. 4. In this experiment, a suspended carbon nanowire deco-

rated with large Pd nanoparticles (NW2) was exposed to 1000 ppm of hydrogen. The wire was heated using via either self-heating or an external heater for 5 s upon closing the hydrogen gas line. The resistance of the composite nanowire recovered faster at higher external heater temperatures. In particular, the resistance completely recovered after a short time with an external heater at 55◦C. Nearly the same resistance recovery behavior was exhibited when the PdNP/carbon nanowire was heated by 30 μW of self-heating. This experiment demonstrates the feasibility of suspended composite nanowires as hydrogen gas sensors capable of complete, instantaneous gas response recovery and precise hydrogen detection, without the signal drift that is frequently exhibited by sensors with slow recovery rates. But, the temperature of PdNP/carbon nanowire heated by 30 μW of self-heating is not 55◦C due to including time (5s) value.

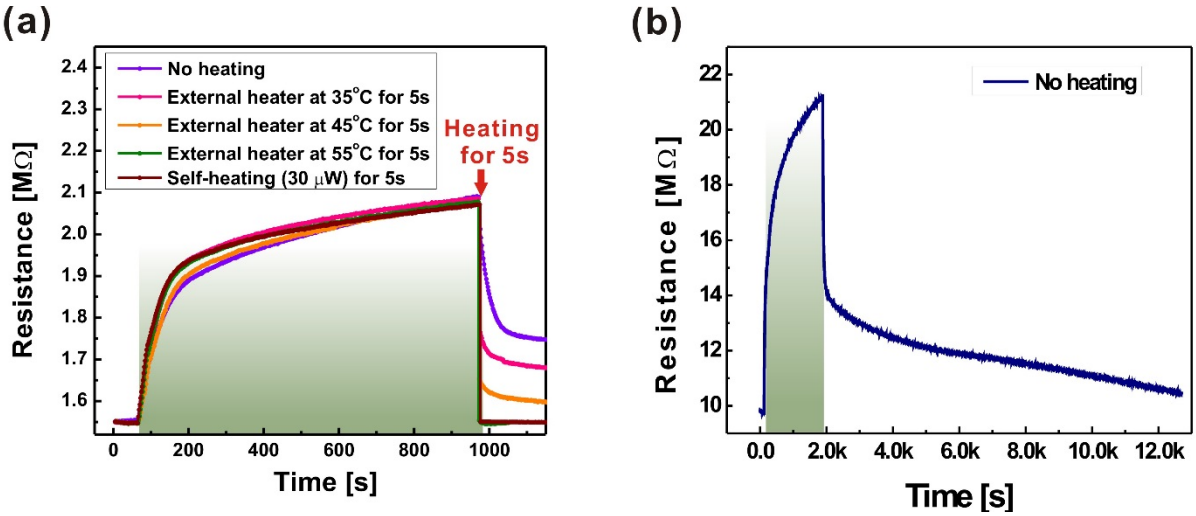

Figure 31. (a) Gas response recovery behavior of NW2 under various heating conditions. The

green shaded area indicates injection of 1,000 ppm of hydrogen. (b) Time consumption graph which show resistance fully recovery at no heating (natural recovery).

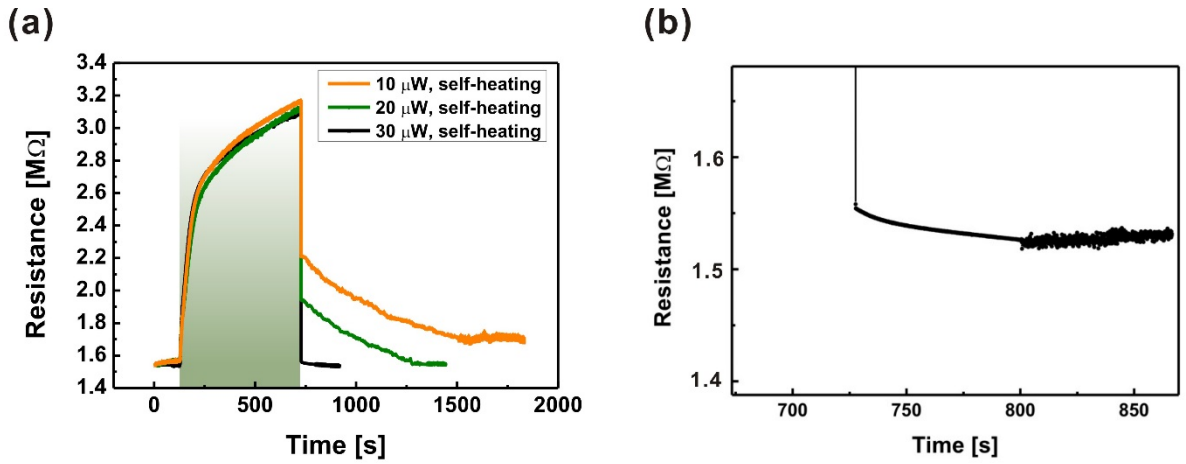

Figure 32. (a) Gas response recovery behavior of NW2 under various self-heating conditions. The green shaded area indicates injection of 1,000 ppm of hydrogen. (b) Magnified part of (a) in 30 μW, self-heating case.

3.3.2 Temperature measurement

In order to exactly calibrate temperature of PdNP/carbon nanowire by self-heating, several experiments are proceeded. First thing is to check simulation result of temperature gradient for same self-heating condition (30 μW). As Figure 33 (a, b), temperature gradient image can be gotten by applied extra power (30 μW) and (c) shows this relationship to point function (Temperature vs. Longitudinal direction). As shown graph, most part of nanowire are heated by 340 K (> 70^{o}C) and temperature of nanowire is rapidly reduced to room temperature. From this result, entire part of nanowire is heated by self-heating (> 70^{o}C) and maximum temperature is 83^{o}C at ceter of nanowire.

And then, the experiment is proceeded which is measuring resistance of nanowire according to increasing temperature of oven because the resistance of nanowire can be increased according to increasing temperature as shown Figure 30 (a). Figure 34 (a) shows schematic image about sample modeling of which the resistance can be measured in oven. Next, the resistance was measured at two environments such as N_2 and Air. But, two environments cannot generate difference because Pd nanomaterial can be oxide (PdO) at over 800^{o}C [37]. And, the resistance of same PdNP/carbon nanowire is measured according to self-heating power (6.25 nW ~ 30 μW). Thus, Figure 35 shows similar phenomenon with oven experiment (heating ↑ → resistance ↑). Lastly, these two graph were matched and as a result, temperature vs. self-heating power can be gotten as shown Figure 36. As Figure 36, the temperature of nanowire is about 70^{o}C and this value is exactly coincident with simulation result.

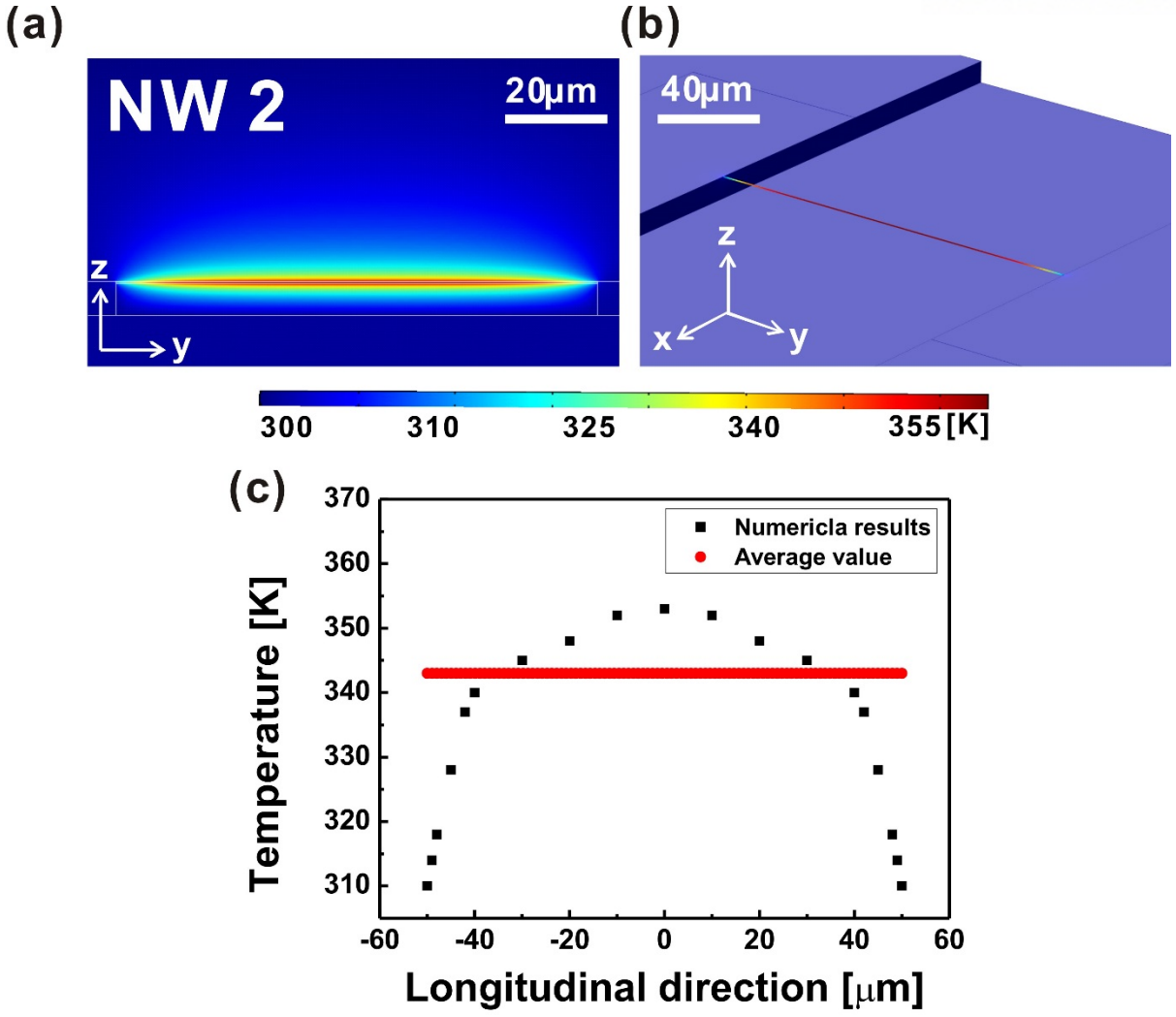

Figure 33. (a, b) Simulation result image for temperature gradient according to self-heating (30 μW). (c) Point function for temperature vs. longitudinal direction of PdNP/carbon nanowire.

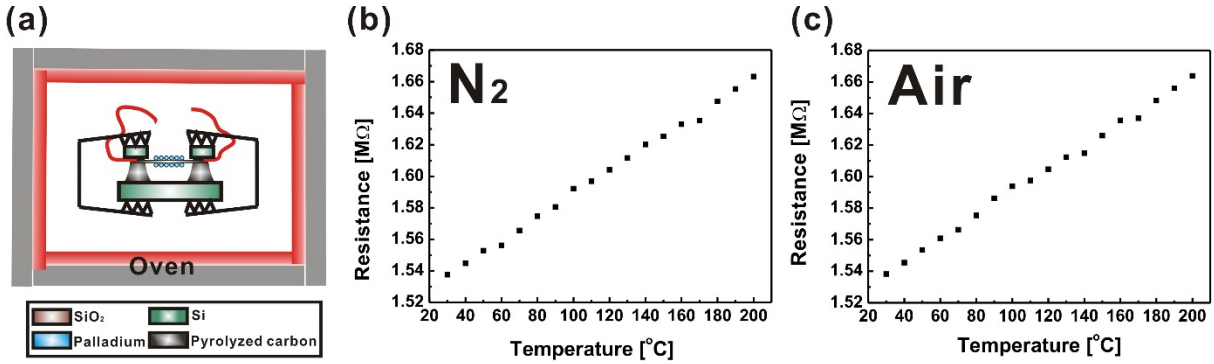

Figure 34. (a) Schematic image: sample modeling of which the resistance can be measured in oven. (b, c) The resistance change according to oven temperature ar N_2 and Air environment.

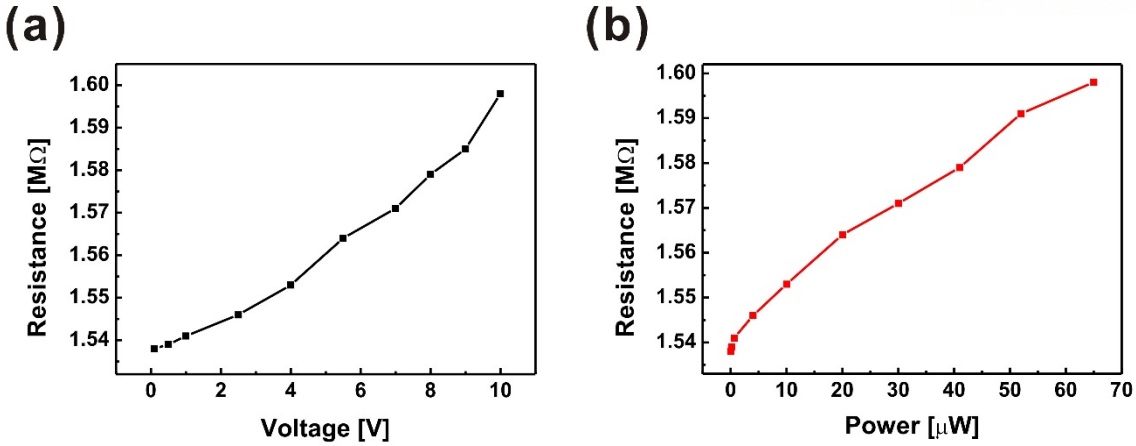

Figure 35. (a, b) The resistance change according to applied voltage and self-heating power of PdNP/carbon nanowire at air environment.

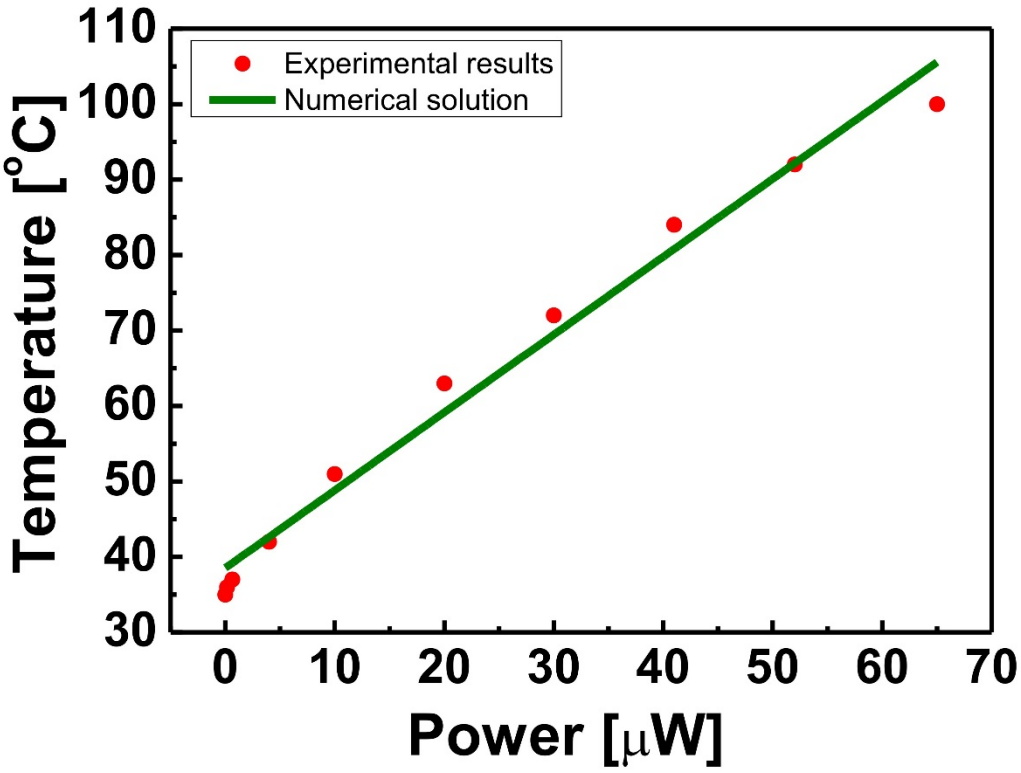

Figure 36. The relation between temperature of PdNP/carbon nanowire and self-heating power. Especially the temperature of PdNP/carbon nanowire is increased by 70°C at 30 μW self-heating.

3.4 Characterization of the hydrogen gas sensing performance

3.4.1 Hydrogen sensing performance

As previously mentioned, Joule-heat-based self-heating is utilized to enhance kinetic interactions between gas molecules and the sensor surface and reduced solubility. Thus, the increase in resistance caused by gas absorption can be recovered instantaneously. Because of the sub-nanoscale diameter of the suspended PdNP/carbon nanowire, and because the delicate nanowire is detached from the substrate, the temperature of PdNP/carbon nanowire can rapidly be increased. However, measurement of changes in the temperatures of the suspended nanowires is limited. Instead, the effect of the self-heating was evaluated by comparing the resistance recovery rates of a suspended PdNP/carbon nanowire under various heating scenarios, as shown in Figure 34-36.

Figure. 37 (a) and (b) show the resistances of NW 1 and NW2 with hydrogen concentrations that vary from 5 % to 10 ppm, at room temperature, with 5 s of ultra-low power (30 μW) self-heating. The composite nanowire with small PdNPs (NW1, Φ 3 – 5 nm) exhibits a larger gas response ($\Delta R/R$; ΔR = change in resistance after hydrogen gas injection, R = resistance before hydrogen gas injection; e.g. $\Delta R/R$ = 185 % at 2.5 % hydrogen) than that ($\Delta R/R$ = 61 % at 2.5 % hydrogen) of the nanowire with large Pd nanoparticles (NW2, Φ 10 – 15 nm). The gas response of NW1 increases quickly for under 1 min and this response correspond linearly with the square root of the hydrogen concentration. However, the response starts to

saturate from 1,000 ppm of hydrogen (Figure 36. (a) and (c)). In contrast, NW2 exhibits a linear gas response from 700 ppm to 5 % of hydrogen (Figure 36. (b) and (c)), in spite of having lower sensitivity than NW1. The sensitivities calculated from linear fitting of the curves in the gas response data are 3.2 % $ppm^{-1/2}$ from 10 − 1,000 ppm and 0.32 % $ppm^{-1/2}$ from 700 ppm − 5 % for NW1 and NW2, respectively. The gas sensing behaviors of the PdNP/carbon-nanowires indicate that sensing capabilities, including sensitivity and sensing range, are closely related to nanoparticle sizes. The resistances of small PdNPs (NW1) increase more quickly with hydrogen injection because of their larger surface to volume ratios. However, the gas response of NW1 becomes saturated at lower concentration (> 1000 ppm)because of the small volume of PdNPs in the composite. In contrast, NW2 exhibits a wider sensing range (10 ppm - 5%) than NW1 which does not exhibit a linear gas response relationship at low hydrogen concentrations. NW2 is not sensitive enough to detect hydrogen at low concentrations because of the small surface to volume ratios induced by large particle sizes.

The linear relationship between the gas response and the square root of hydrogen concentration can be understood by applying the Langmuir adsorption isotherm theory to dissociation of hydrogen molecules upon catalyst and adsorption reaction on the Pd nanoparticle surface [38]. hydrogen dissociation on Pd nanoparticle surface can be described via Equation (1).

$$\text{hydrogen} + 2Pd \leftrightarrow 2PdHx \quad (1)$$

The adsorption and desorption rates of hydrogen can be expressed as $k_1 p(1-\theta)^2$ and $k_{-1}\theta^2$ where k_1 and k_{-1} are the adsorption and desorption constants, respectively. In these expressions, p is the partial pressure of hydrogen and θ is the fraction occupied by adsorbed hydrogen in Pd surface sites. At equilibrium, the adsorption and desorption rates are equal, and thus the ratio of the occupied to non-occupied surface sites is proportional to the square root of the partial pressure. This is described in Equation (2).

$$k_1 p(1-\theta)^2 = k_{-1}(\theta)^2 \quad \text{or} \quad \frac{\theta}{1-\theta} = \left(\frac{k_1}{k_{-1}}\right)^{1/2} p^{1/2} \tag{2}$$

At low concentrations of hydrogen ($\theta << 1$), the ratio of occupied to non-occupied surface sites is proportional to the square root of the partial pressure or concentration of hydrogen. Therefore, it can be concluded that the gas response of the PdNP/carbon nanowire is closely related to chemisorption, as described by Equation (3):

$$\Delta R / R \propto \theta \approx (k_1 / k_{-1})^{1/2} p^{1/2} \tag{3}$$

The response times of NW1 and NW2 at various hydrogen concentrations are shown in Figure 36. (d). The response time is defined as the time required for the sensor to reach e^{-1} (~36.8 %) of the maximum resistance change after hydrogen exposure [39, 40]. Both types of composite nanowires (NW1 and NW2) show fast gas responses at room temperature (< 1 min) due to high surface to volume ratio. At low gas concentrations, θ is insignificant so the

adsorption rate is linearly proportional to the gas concentration. The adsorption rate is then gradually affected by the $(1 - \theta)^2$ term as the gas concentration increases. Thus, the initial response time is inversely proportional to the gas concentration. The response time curve of NW1 exhibits good agreement with this inverse relationship at low concentrations (10 – 1,000 ppm), but the gas response time gradually increases with the gas concentration because the surface sites available for hydrogen adsorption become depleted. However, the composite nanowire decorated with large PdNPs (NW2) exhibits an inverse relationship at relatively high gas concentrations (700 ppm – 5 %) because of its long diffusion path and small surface area to volume ratio. At hydrogen concentrations lower than 1,000 ppm, NW1 responds faster than NW2. This relationship is reversed at high hydrogen concentrations (> 1,000 ppm). With small Pd nanoparticles, hydrogen diffusion into bulk Pd occurs efficiently, even at low gas concentrations because of the large surface area to volume ratios property. However, the Pd particles easily become saturated with hydrogen because of their small size. Large Pd nanoparticles exhibit low gas responses because of their relatively small surface area to volume ratios, but saturation is delayed (> 5%) because the particles are larger.

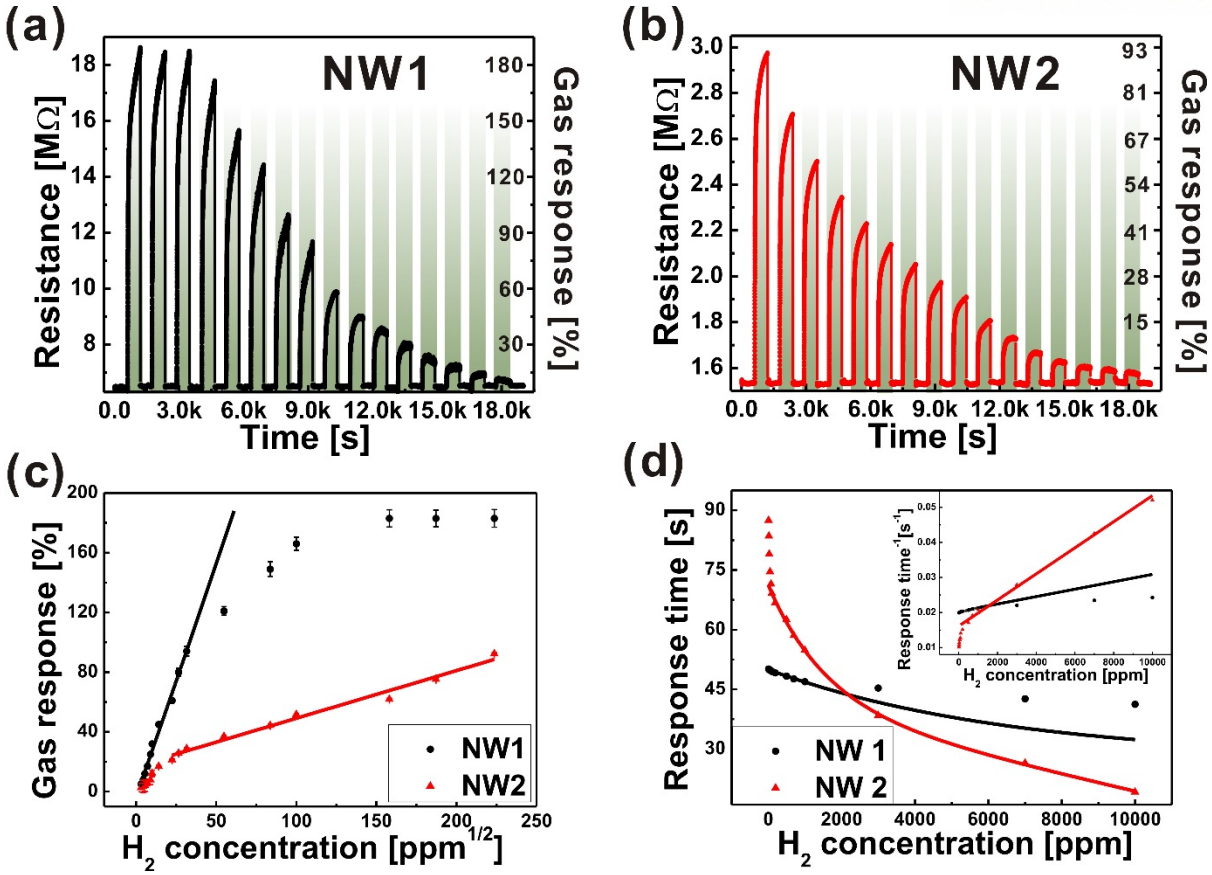

Figure 36. Eelectrical resistance and gas response graphs of PdNP/carbon nanowires ((a) NW1, PdNPs size: 3 – 5 nm, (b) NW2, PdNPs size: 10 – 15 nm) with various concentration amounts of hydrogen (green shaded blocks indicate 5, 3.5, 2.5, 1, 0.7, and 0.3 %, and 1,000, 700, 500, 200, 100, 80, 50, 30, 20, and 10 ppm respectively) mixed with air at room temperature. (c) Gas responses of NW1 and NW2 versus the square root of hydrogen concentration. (d) Response time versus hydrogen concentration. The inset graph shows the reciprocal of response time vs. hydrogen concentration.

3.4.2 Reproducible and long term durability

The reproducibility and reliability of the PdNP/carbon-nanowire-based hydrogen gas sensors were evaluated by cycling hydrogen gas injection and purging steps with various gas concentrations, as shown in Fig. 7. Both NW1 and NW2 exhibited similar gas responses at the same hydrogen concentrations after several gas injection cycles. This indicates the ability of

the gas sensors to provide precise, continuous detection of hydrogen gas concentrations.

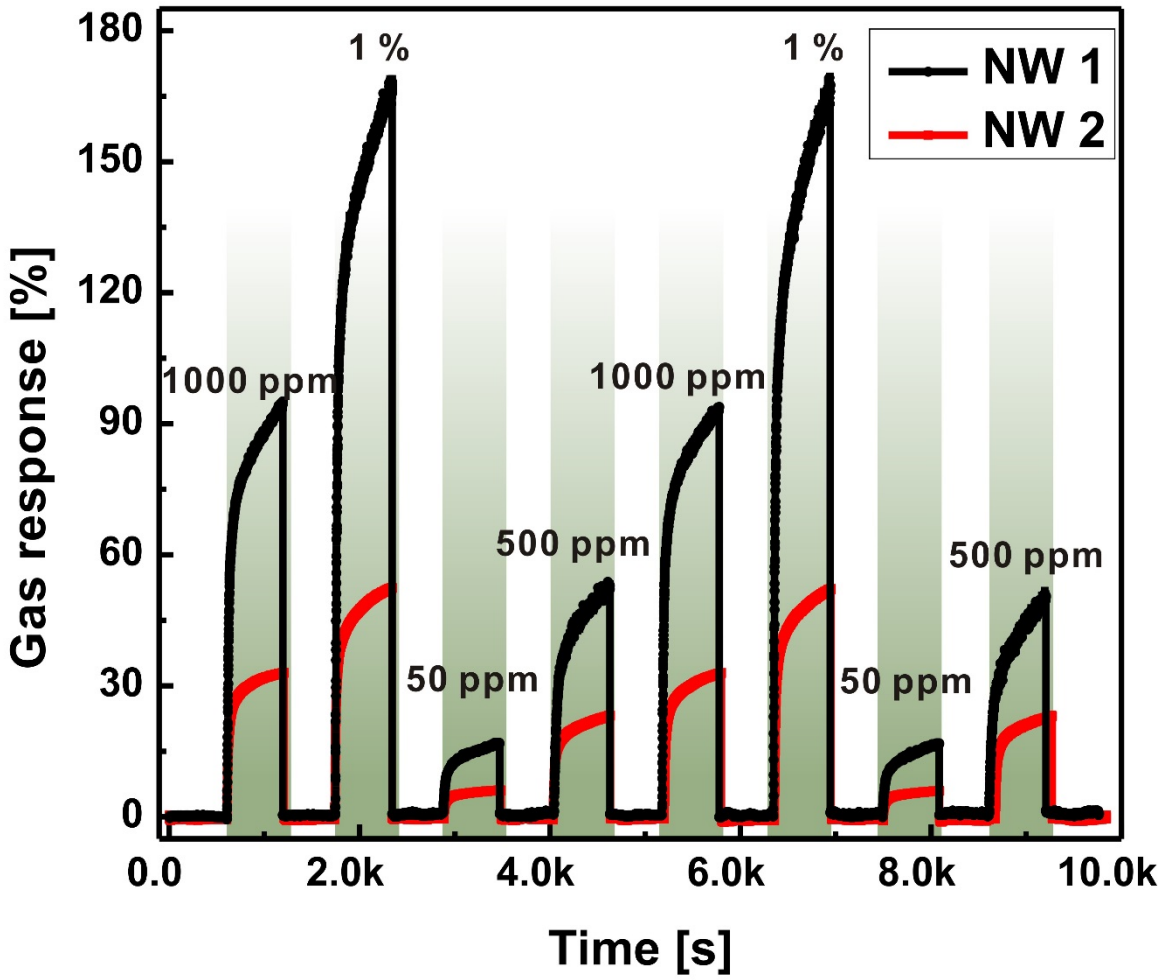

Figure 37. Reproducible gas responses of suspended PdNP/carbon nanowires (NW1, PdNPs diameter: 3 – 5 nm, (b) NW2, PdNPs diameter: 10 – 15 nm) during several injection-purging cycles with randomly concentrations of hydrogen.

The long-term durability of the gas sensor was tested by cycling injection of hydrogen to the gas sensor for 30 days without self-heating. As previously mentioned, complete recovery of the gas response requires significant time because of slow solid diffusion at room temperature. In addition, humidity and contaminants deplete the available Pd surface sites and thus the gas response reduces as the operating time increases [30]. NW1 exhibits the same

sensor signal degradation, as shown in Fig. 8. However, application of 5 s of self-heating to the composite nanowire completely recovers its gas response capability, even after 30 days of sensor operation.

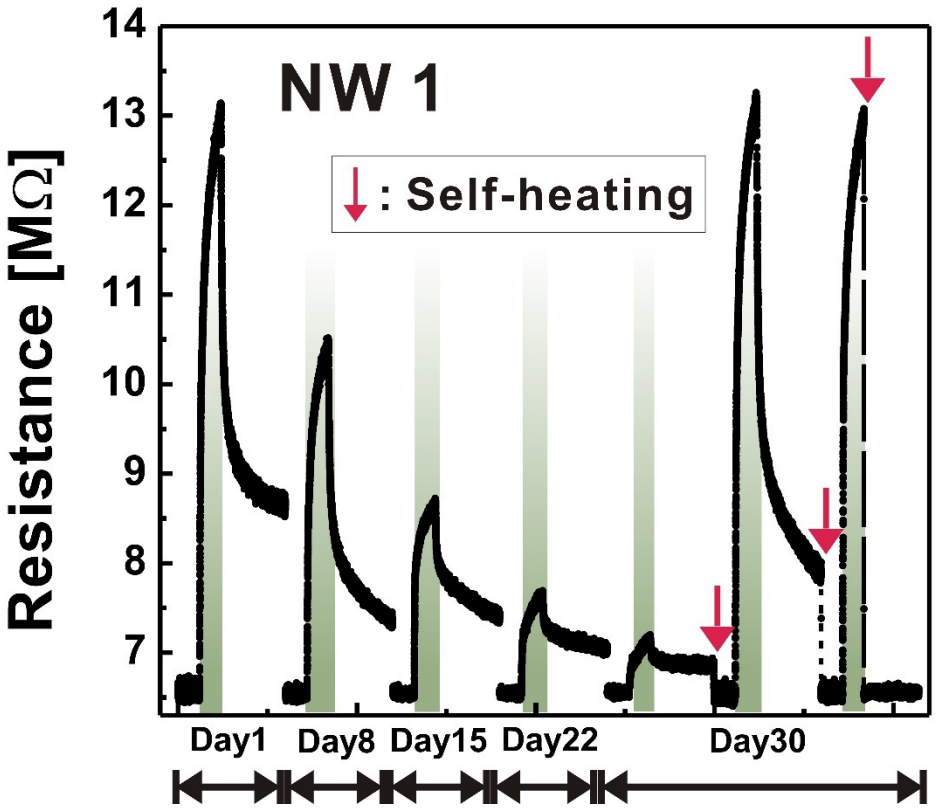

Figure 38. Long-term durability experiment was shown via the gas response and recovery behaviors of NW1 (diameter: 3 – 5 nm) tested once a day in the period of 30 day. Green shaded areas present the injection of 1,000 ppm of hydrogen. Red arrows present self-heating for 5 s.

3.4.3 Gas response improvement

The gas response is continuously increased at 6.25 nW applied power when 1000 ppm hydrogen injected as shown Figure 39 black line. In this case, exact hydrogen concentration calibration can be impossible at real sensing environment due to changeable gas response. However, this problem can be solved by continuous self-heating not spontaneous self-heating (5s). As shown Figur 39, green line show saturation phenomenon with low gas response and pink line show quickly saturated gas response (< 5s) due to low gas solubility and fast kinetic hydrogen molecules. Therefore, continuous heating facilitates exact hydrogen concentration calibration.

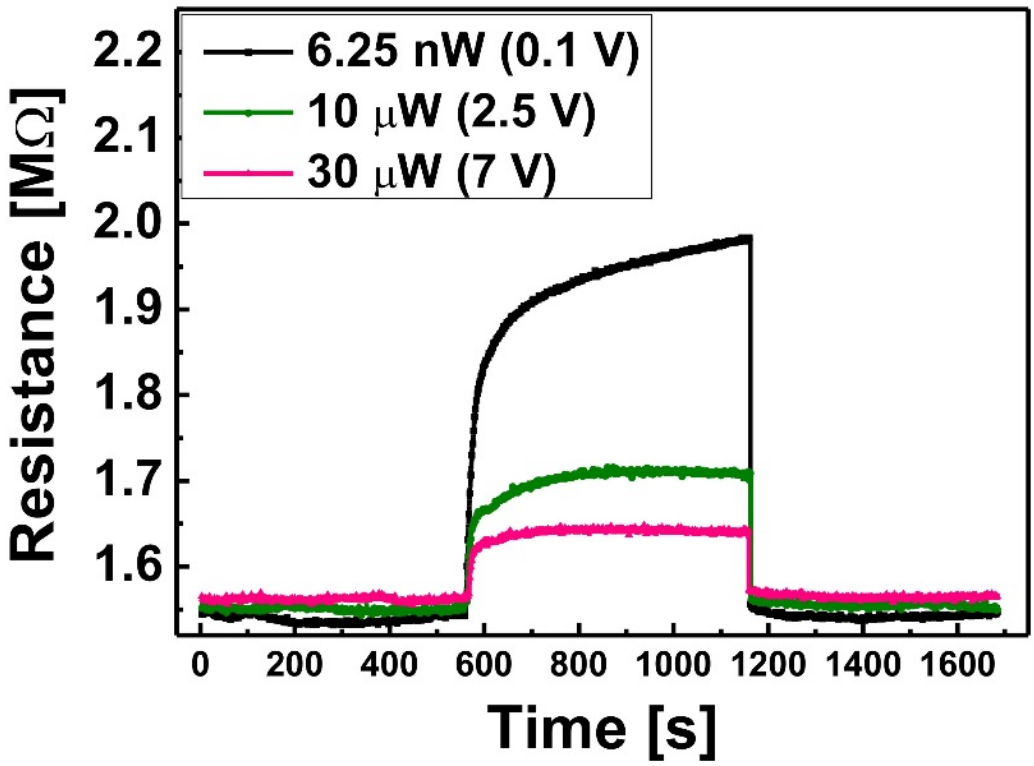

Figure 39. Gas responses of suspended PdNP/carbon nanowires (NW2, PdNPs diameter: 10 – 15 nm) according to continuous heating power. In continuous self-heating (30 μW), gas response time is under 2s like pink line.

4. Conclusion

We have developed a novel gas sensor based on an array of individual, suspended carbon nanowires decorated with PdNPs of various sizes for room temperature hydrogen gas sensing with high sensitivity, a wide sensing range (10 ppm − 5 %), and complete recovery in 5 s via low power consumption self-heating. These suspended PdNP/carbon nanowires were fabricated using conventional batch microfabrication methods including carbon-MEMS and electrodeposition. The electrical resistances of PdNP/carbon nanowires were dominated by the PdNPs because charge carriers flow preferentially via PdNPs due to the relatively low electrical conductivities of the carbon nanowires. The sensitivity and linear sensing range of the hydrogen sensor were modulated by controlling the sizes of the PdNPs. Thus, a wide range of hydrogen gas sensing capabilities can be facilitated by building an array of single suspended carbon nanowires integrated with PdNPs of various sizes. Furthermore, due to their suspended architecture, the resistances of the PdNP/carbon nanowires were quickly and completely recovered via ultra-low-power, Joule heat-based self-heating. This unique sensing capability also enabled reproducible, reliable, long-term, and durable hydrogen gas sensing. Such good room temperature gas sensing performance has not been reported thus far. The hydrogen gas sensors exhibit excellent feasibility as a high performance hydrogen detection and monitoring tools with the advantages of low power, continuous sensing without calibration, a wide sensing range, high sensitivity, and cost-effective fabrication.

Reference

[1] K. Agbossou, R. Chahine, J. Hamelin, F. Laurencelle, A. Anouar, J.-M. St-Arnaud, T.K. Bose, "Renewable energy systems based on hydrogen for remote applications", *J. Power Sources*, **96**, 168-172 (2001).

[2] V. A. Goltsov, T. Nejat Veziroglu, "A step on the road to hydrogen civilization", *Int. J. Hydrogen Energy*, **27**, 719-723 (2002).

[3] M. Z. Jacobson, W. G. Colella, D. M. Golden, "Cleaning the air and improving health with hydrogen fuel-cell vehicles", *Science*, **308**, 1901-1905 (2005).

[4] T. Hubert, L. Boon-Brett, G. black, U. Banach, "Hydrogen sensors – A review", *Sens. Actuator B-Chem.*, **157**, 329-352 (2011).

[5] X. Chen, C. K. Y. Wong, C. A. Yuan, G. Zhang, "Nanowire-based gas sensors", *Sens. Actuator B-Chem.*, **177**, 178-195 (2013).

[6] E. R. Waclawik, J. Chang, A. Ponzoni, I. Concina, D. Zappa, E. Comini, N. Motto, G. Faglia, G. Sberveglieri, "Functionalized zinc oxide nanowire gas sensors: Enhanced NO2 gas sensor response by chemical modification of nanowire surfaces", *Beilstein J. Nanotechnol.*, **3**, 368-377 (2012).

[7] F. Hernandez-Ramirez, J. D. Prades, J. R. Morante, "Metal oxide nanowire gas sensors", *Sensor Mater.*, **21**, 219-227 (2009).

[8] S. Mubeen, T. Zhang, B. Yoo, M. A. Deshusses, N. V. Myung, "Palladium nanoparticles decorated single-walled carbon nanotube hydrogen sensor", *J. Phys. Chem.*, **111**, 6321-6327 (2007).

[9] H. Huang, Y. Lee, O. Tan, W. Zhou, N. Peng, Q. Zhang, "High sensitivity SnO_2 single-nanorod sensors for the detection of hydrogen gas at low temperature", *Nanotechnology*, **20**, 115501-115506 (2009).

[10] M U. Lange, T. Hirsch, V. M. Mirsky, O.S. Wolfbeis, "Hydrogen sensor based on a graphene -palladium nanocomposite", *Electrochim. Acta.*, **56**, 3707-3712 (2011).

[11] E. Lee, J. Lee, J. Koo, W. Lee, T. Lee, "Hysteresis behavior of electrical resistance in Pd thin films during the process of absorption and desorption of hydrogen gas", *Int. J. Hydrogen Energy*, **35**, 6984-6991 (2010).

[12] A.L. Cabrera, R. Aguayo-Soto, "Hydrogen absorption in palladium films sensed by changes in their resistivity", *Catal. Lett*., **45**, 79-83 (1997).

[13] S. Nakano, S.-I. Yamaura, S. Uchinashi, H. Kimura, A. Inoue, "Effect of hydrogen on the electrical resistance of melt spum $Mg_{90}Pd_{10}$ amorphous alloy", *Sens. Actuator B-Chem.*, **104**, 75-79 (2005).

[14] M. Wang, Y. Feng, "Palladium-silver thin film for hydrogen sensing", *Sens. Actuator B-Chem.*, **123**, 101-106 (2007).

[15] E. Lee, J. Lee, E. Lee, J.-S. Noh, J. Joe, B. Jung, W. Lee, "Hydrogen gas sensing performance of Pd-Ni alloy thin films", *Thin Solid Films*, **519**, 880-894 (2010).

[16] D. Ding, Z. Chen, C. Lu, "Hydrogen sensing of nanoporous palladium films supported by anodic aluminum oxides", *Sens. Actuator B-Chem.,* **120**, 182-186 (2006).

[17] J. Choi, J. Kim, "Highly sensitive hydrogen sensor based on suspended, functionalized single tungsten nanowire bridge", *Sens. Actuator B-Chem.*, **136**, 92-98 (2009).

[18] P. Offermans, H. D. Tong, C. J. M. van Rijn, P. Merken, S. H. Brongersma, M. Crego-Calama, "Ultralow-power hydrogen sensing with single palladium nanowires", *Appl. Phys. Lett.*, **94**, 223110-223113 (2009).

[19] E.C. Walter, F. Favier, R.M. Penner, "Palladium mesowire arrays for fast hydrogen sensors and hydrogen actuated switches", *Anal. Chem.,* **47**, 1546-1553 (2002).

[20] J.-S. Noh, H. Kim, B. Kim, E. Lee, H. Cho, W. Lee, "High-performance vertical hydrogen sensors using Pd-coated rough Si nanowires", *J. Mater. Chem.*, **21**, 15935-15939 (2011).

[21] R. K. Joshi, S. Krishnan, "Pd nanoparticles and thin films room temperature hydrogen sensor", *Nanoscale Res. Lett.*, **4**, 1191-1196 (2009).

[22] Y. Lim, Y. Lee, J.-I. Heo, H. Shin, "Highly sensitive hydrogen gas sensor based on a suspended palladium/carbon nanowire fabricated via batch microfabrication processes", *Sens. Actuator B-Chem.*, **210**, 218-224 (2015).

[23] F. Yang, D. K. Taggart, R. M. Penner, "Joule heating a palladium nanowire sensor for accelerated response and recovery to hydrogen gas", *Small*, **13**, 1422-1429 (2010).

[24] J. Yun, C. Jin, J.-H. Ahn, S. Jeon, I. Park, "A self-heated silicon nanowire array: selective surface modification with catalytic nanoparticles by nanoscale joule heating and its gas sensing applications", *Nanoscale*, **5**, 6851-6856 (2013).

[25] J.-H. Ahn, J. Yun, D.-I. Moon, Y.-K. Choi, I. Park, "Self-heated silicon nanowires for high performance hydrogen gas detection", *Nanotechnology,* **26**, 095501-095510 (2015).

[26] K. Chikkadi, M. Muoth, V. Maiwald, C. Roman, C. Hierold, "Ultra-low power operation of self-heated, suspended carbon nanotube gas sensors", *Appl. Phys. Lett.,* **103**, 223109 (2013).

[27] O. Lupan, V. Postica, M. Mecklenburg, K. Schulte, Y. K. Mishra, B. Fiedler, R. Adelung, "Low powered, tunable and ultra-light aerographite sensor for climate relevant gas monitoring", *J. Mater. Chem. A*, **4**, 16723 (2016).

[28] C. M. Lentz, B. A. Samuel, H. C. Foley, M. A. Haque, "Synthesis and characterization of glassy carbon nanowires", *J. Nanomater.*, 129298 (2011).

[29] Y. Lim, J.-I. Heo, M. Madou, H. Shin, "Monolithic carbon structures including suspended single nanowires and nanomeshes as a sensor platform", *Nanoscale Res. Lett.,* **8**, 492-501 (2013).

[30] F. A. Lewis, "The palladium-hydrogen system", *Platin. Net. Rev.*, **26**, 121-128 (1982).

[31] M. Chung, D.-H. Kim, D. Seo, T. Kim, H. Im, H. Lee, J.-B. Yoo, S.-H. Hong, T. Kang, Y. Kim, "Flexible hydrogen sensors using graphene with palladium nanoparticle decoration", *Sens. Actuator B-Chem.*, **169**, 387-392 (2012).

[32] V. Palmisano, E. Weidner, L. Boon-Brett, C. Bonato, F. Harskamp, P. Moretto, M.B. Post, R. Burgess, C. Rivkin, W.J. Buttner, "Selective and resistance to poisons of commercial hydrogen sensors", *Int. J. Hydrogen Energy,* **40**, 11740-11747 (2015).

[33] S. Kabcum, D. Channeib, A. Tuantranontc, A. Wisitsoraatc, C. Liewhirana, S. Phanichphant, "Ultra-responsive hydrogen gas sensors based on PdO nanoparticle-decorated WO_3 nanorods synthesized by precipitation and impregnation methods", *Sens. Actuators B-Chem.*, **226**, 76-89 (2016).

[34] Z. Abideen, H. Kim, S. Kim, "An ultra-sensitive hydrogen gas sensor using reduced graphene oxide-loaded ZnO nanofibers", *Chem. Commun.*, **51**, 15418-15421 (2015).

[35] J. Lee, J.-E. Park, S. Kim, S. Kim, E. Lee, S.-J. Kim, W. Lee, "Ultra-sensitive hydrogen gas sensors based on Pd-decorated tin dioxide nanostructures: Room temperature operating sensors", *Int. J. Hydrogen Energy*, **35**, 12568-12573 (2010).

[36] P.A. Russo, N. Donato, S.G. Leonardi, S. Baek, D.E. Conte, G. Neri, N. Pinna, "Room-temperature hydrogen sensing with heteronanostructures based on reduced graphene oxide and tin oxide", *Sensors*, **51**, 11053-11057 (2012).

[37] Y. Sun, H.H. Wang, "High-performance, flexible hydrogen sensors that use carbon nanotubes decorated with palladium nanoparticles", *Adv. Mater.,* **19**, 2818-2823 (2007).

[38] J.L. Johnson, A. Behnam, S.J. Pearton, A. Ural, "Hydrogen sensing using Pd functionalized multi-layer graphene nanoribbon networks", *Adv. Mater.*, **22**, 4877-4880 (2010).

[39] R.D. Martinez-Orozco, R. Antano-Lopez, V. Rodriguez-Gonzalez, "Hydrogen-gas sensors based on graphene functionalized palladium nanoparticles: impedance response as a valuable sensor", *New J. Chem.*, **39**, 8044-8054 (2015).

[40] D. Shin, J. Lee, J. Jun, J. An, S. Kim, K. Cho, J. Jang, "Flower-like palladium nanoclusters decorated graphene electrodes for ultrasensitive and flexible hydrogen gas sensing", *Sci. Rep.*, **5**, 12294 (2015).

[41] A.L. Cabrera, R. Aguayo-Soto, "Hydrogen absorption in palladium films sensed by changes in their resistivity", *Catal. Lett*., **45**, 79-83 (1997).

[42] S. Nakano, S.-I. Yamaura, S. Uchinashi, H. Kimura, A. Inoue, "Effect of hydrogen on the electrical resistance of melt spum $Mg_{90}Pd_{10}$ amorphous alloy", *Sens. Actuator B-Chem.*, **104**, 75-79 (2005).

[43] M. Wang, Y. Feng, "Palladium-silver thin film for hydrogen sensing", *Sens. Actuator B-Chem.*, **123**, 101-106 (2007).

[44] E. Lee, J. Lee, E. Lee, J.-S. Noh, J. Joe, B. Jung, W. Lee, "Hydrogen gas sensing performance of Pd-Ni alloy thin films", *Thin Solid Films*, **519**, 880-894 (2010).

[45] D. Ding, Z. Chen, C. Lu, "Hydrogen sensing of nanoporous palladium films supported by anodic aluminum oxides", *Sens. Actuator B-Chem.,* **120**, 182-186 (2006).

[46] J. Choi, J. Kim, "Highly sensitive hydrogen sensor based on suspended, functionalized single tungsten nanowire bridge", *Sens. Actuator B-Chem.*, **136**, 92-98 (2009).

[47] P. Offermans, H. D. Tong, C. J. M. van Rijn, P. Merken, S. H. Brongersma, M. Crego-Calama, "Ultralow-power hydrogen sensing with single palladium nanowires", *Appl. Phys. Lett.*, **94**, 223110-223113 (2009).

[48] E.C. Walter, F. Favier, R.M. Penner, "Palladium mesowire arrays for fast hydrogen sensors and hydrogen actuated switches", *Anal. Chem.,* **47**, 1546-1553 (2002).

[49] T. Hubert, L. Boon-Brett, G. black, U. Banach, "Hydrogen sensors – A review", *Sens. Actuator B-Chem.*, **157**, 329-352 (2011).

[50] X. Chen, C. K. Y. Wong, C. A. Yuan, G. Zhang, "Nanowire-based gas sensors", *Sens. Actuator B-Chem.*, **177**, 178-195 (2013).

[51] E. R. Waclawik, J. Chang, A. Ponzoni, I. Concina, D. Zappa, E. Comini, N. Motto, G. Faglia, G. Sberveglieri, "Functionalized zinc oxide nanowire gas sensors: Enhanced NO2 gas sensor response by chemical modification of nanowire surfaces", *Beilstein J. Nanotechnol.*, **3**, 368-377 (2012).

[52] F. Hernandez-Ramirez, J. D. Prades, J. R. Morante, "Metal oxide nanowire gas sensors", *Sensor Mater.*, **21**, 219-227 (2009).

[53] S. Mubeen, T. Zhang, B. Yoo, M. A. Deshusses, N. V. Myung, "Palladium nanoparticles decorated single-walled carbon nanotube hydrogen sensor", *J. Phys. Chem.*, **111**, 6321-6327 (2007).

[54] H. Huang, Y. Lee, O. Tan, W. Zhou, N. Peng, Q. Zhang, "High sensitivity SnO_2 single-nanorod sensors for the detection of hydrogen gas at low temperature", *Nanotechnology*, **20**, 115501-115506 (2009).

[55] M U. Lange, T. Hirsch, V. M. Mirsky, O.S. Wolfbeis, "Hydrogen sensor based on a graphene -palladium nanocomposite", *Electrochim. Acta.*, **56**, 3707-3712 (2011).

[56] F. Yang, D. K. Taggart, R. M. Penner, "Joule heating a palladium nanowire sensor for accelerated response and recovery to hydrogen gas", *Small*, **13**, 1422-1429 (2010).

[57] J. Yun, C. Jin, J.-H. Ahn, S. Jeon, I. Park, "A self-heated silicon nanowire array: selective surface modification with catalytic nanoparticles by nanoscale joule heating and its gas sensing applications", *Nanoscale*, **5**, 6851-6856 (2013).

[58] J.-H. Ahn, J. Yun, D.-I. Moon, Y.-K. Choi, I. Park, "Self-heated silicon nanowires for high performance hydrogen gas detection", *Nanotechnology,* **26**, 095501-095510 (2015).

[59] K. Chikkadi, M. Muoth, V. Maiwald, C. Roman, C. Hierold, "Ultra-low power operation of self-heated, suspended carbon nanotube gas sensors", *Appl. Phys. Lett.,* **103**, 223109 (2013).

[60] O. Lupan, V. Postica, M. Mecklenburg, K. Schulte, Y. K. Mishra, B. Fiedler, R. Adelung, "Low powered, tunable and ultra-light aerographite sensor for climate relevant gas monitoring", *J. Mater. Chem. A*, **4**, 16723 (2016).

Acknowledgements

I deeply thanks to my advisor, Professor Heungjoo Shin. He always guided me to improve my research with wisdom from internship program to the master's course. Without his guidance and supports, I couldn't experience research life and finish this thesis. I want to say the appreciation but my late. I also appreciate to the committee members, Professor Taesung Kim and Professor Hoon Eui Jeong for giving suggestions and assistances during the thesis presentation. Thanks to them, I could successfully complete this thesis.

And I want to give thanks to all MNIS Lab members, Deepti Sharma, Yeongjin Lim, Jongmin Lee, Jisoo Hong, Soosung kim, Beomsang Kim, Seungwook Lee and our baby, Taejung Kim. Owing to their helps, I could finish my master course and spend happy and joyful time during master's course in UNIST. Spatially, to my sister, Jisoo Hong and my little brother, Soosung Kim, I'm thankful for continuous trust. Moreover, I also want to say thank to Microfludics/Nanomechatronics (μFNM) lab members who spent much time to talk and drink with me. And, I want to give thanks to Chang-Ho Han for visiting my thesis presentation who is in Sensors & Aerosols Lab. Owing to advises of my friends, Junghyun Lee and Jaegi Lee, I could decide my way in future life. I also extend to express the thanks to Sanga Park, Hyun-Ha Park, Hangil Ko, Jiyun Jeon and Chanbeom Bak. Above them, I want to express the thanks to my forever friends, SSEURAEGITONG including Gihoon Kang, Heechang Kim, Bosu Kim, Jaehong Kwon, Jinseong Kim, Jeonghyun Kim, Dongkyu Kim and Jungwon Choi who are the greatest gift in my life. Lastly, thanks to Sohee Park who is administrate teacher for always helping to complete master's course.

Whenever I was depressed, my family have always trusted me and given infinite trust and love. Owing to their dedication like confidence from my father, gentle love from my mother, courage from my sister and great concerns from my aunts, uncles, and cousins, I could finish master's course. I sincerely appreciate to them. Finally, I want to express appreciation to my Soojin Kim for her dedication and endless love. I would not forget your love forever. Make each day count!